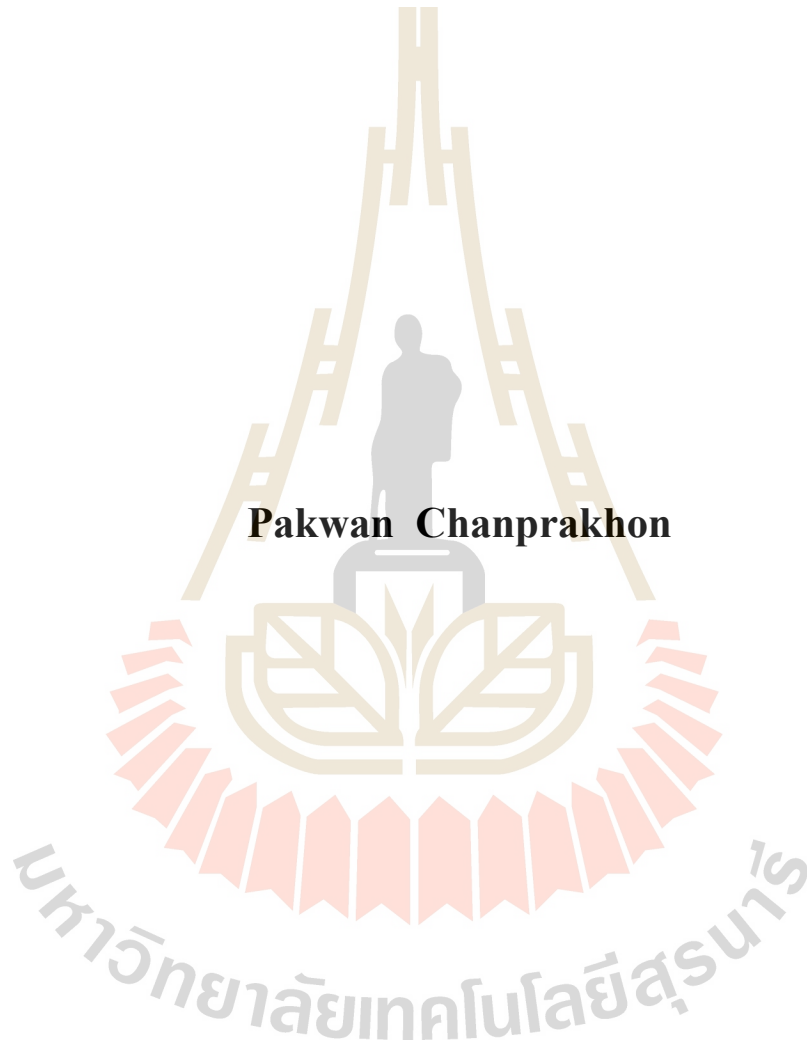


**ELECTRONIC STRUCTURE OF OPTICALLY EXCITED  
MOLYBDENUM DISULFIDE SINGLE CRYSTALS**



**Pakwan Chanprakhon**

**A Thesis Submitted in Partial Fulfillment of the Requirement for the**

**Degree of Master of Science in Physics**

**Suranaree University of Technology**

**Academic Year 2019**

โครงสร้างทางอิเล็กทรอนิกส์ของผลึกเดี่ยวโพลีบดึ้นมไดซัลไฟด์ที่ถูกระตุ้น  
เชิงแสง



นางสาวพาขวัญ ชาญประโคน

วิทยานิพนธ์นี้เป็นส่วนหนึ่งของการศึกษาตามหลักสูตรปริญญาวิทยาศาสตรมหาบัณฑิต

สาขาวิชาฟิสิกส์

มหาวิทยาลัยเทคโนโลยีสุรนารี

ปีการศึกษา 2562

**ELECTRONIC STRUCTURE OF OPTICALLY EXCITED  
MOLYBDENUM DISULFIDE SINGLE CRYSTALS**

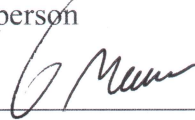
Suranaree University of Technology has approved this thesis submitted in partial fulfillment of the requirements for a Master's degree.

Thesis Examining Committee



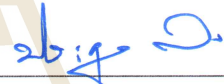
(Asst. Prof. Dr. Panomsak Meemon)

Chairperson




(Assoc. Prof. Dr. Worawat Meevasana)

Member (Thesis Advisor)



(Assoc. Prof. Dr. Prayoon Songsirithigul)

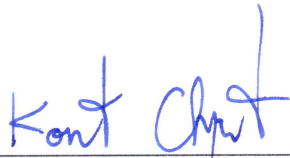
Member



(Dr. Hideki Nakajima)

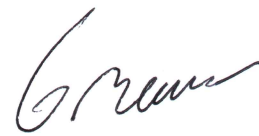
Member

มหาวิทยาลัยเทคโนโลยีสุรนารี



(Assoc. Prof. Ft. Lt. Dr. Kontorn Chamniprasart)

Vice Rector for Academic Affairs  
and Internationalization



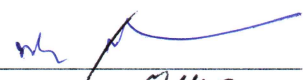
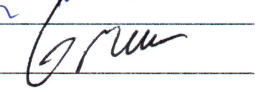
(Assoc. Prof. Dr. Worawat Meevasana)

Dean of Institute of Science

พาวณีย์ ชามูประโคน : โครงสร้างทางอิเล็กทรอนิกส์ของผลึกเดี่ยวโมลิบดีนัมไดซัลไฟด์ที่  
ถูกกระตุ้นเชิงแสง (ELECTRONIC STRUCTURE OF OPTICALLY EXCITED  
MOLYBDENUM DISULFIDE SINGLE CRYSTALS). อาจารย์ที่ปรึกษา :  
รองศาสตราจารย์ ดร. วรวัฒน์ มีวาสนา, 54 หน้า.

โมลิบดีนัมไดซัลไฟด์เป็นวัสดุที่เป็นที่รู้จักซึ่งได้รับการศึกษาเพื่อใช้ในอุปกรณ์อิเล็กทรอนิกส์เนื่องจากมีคุณสมบัติทางอิเล็กทรอนิกส์ที่น่าสนใจซึ่งสัมพันธ์กับโครงสร้างทางอิเล็กทรอนิกส์ เทคนิคโฟโตอิมชันแบบแยกแยะเชิงมุมเป็นเทคนิคที่สามารถวัดโครงสร้างทางอิเล็กทรอนิกส์ของสารได้โดยตรง ในงานนี้ได้ทำการศึกษาโครงสร้างทางอิเล็กทรอนิกส์ของผลึกเดี่ยวโมลิบดีนัมไดซัลไฟด์ที่ถูกกระตุ้นด้วยแสงจากเลเซอร์ในโมลิบดีนัมไดซัลไฟด์บริสุทธิ์และโมลิบดีนัมไดซัลไฟด์ที่ถูกเจือด้วยโพแทสเซียมโดยใช้เทคนิคโฟโตอิมชันแบบแยกแยะเชิงมุม โดยในโมลิบดีนัมไดซัลไฟด์บริสุทธิ์ พบว่าแถบวาเลนซ์ของโมลิบดีนัมไดซัลไฟด์มีการขยับไปทางพลังงานยึดเหนี่ยวที่สูงขึ้นเมื่อถูกฉายด้วยแสงเลเซอร์ซึ่งเป็นผลมาจากการที่อิเล็กตรอนในแถบวาเลนซ์ถูกกระตุ้นให้ไปอยู่ที่แถบนำไฟฟ้า สำหรับในโมลิบดีนัมไดซัลไฟด์ที่ถูกเจือด้วยโพแทสเซียมพบว่าแถบวาเลนซ์มีการขยับไปทางพลังงานยึดเหนี่ยวที่สูงขึ้นเมื่อเทียบกับโมลิบดีนัมไดซัลไฟด์บริสุทธิ์ซึ่งเป็นผลมาจากการให้อิเล็กตรอนจากโพแทสเซียมไปที่โมลิบดีนัมไดซัลไฟด์ซึ่งสอดคล้องกับการพบก่อนของอิเล็กตรอนที่แถบนำไฟฟ้า เมื่อฉายแสงลงบนโมลิบดีนัมไดซัลไฟด์ที่ถูกเจือด้วยโพแทสเซียมยังคงพบการขยับของแถบวาเลนซ์หลังจากที่ถูกกระตุ้นด้วยแสงเลเซอร์ซึ่งสามารถอธิบายได้ว่าอิเล็กตรอนที่แถบวาเลนซ์ยังคงถูกกระตุ้นด้วยแสงไปที่แถบนำไฟฟ้าในโมลิบดีนัมไดซัลไฟด์ที่ถูกเจือ การขยับของแถบวาเลนซ์ทั้งหมดที่เกิดขึ้นสามารถอธิบายได้ด้วยโมเดลของแผนภาพโครงสร้างอิเล็กทรอนิกส์ของโมลิบดีนัมไดซัลไฟด์และตำแหน่งของระดับพลังงานเฟอร์มีที่แตกต่างกัน จากการวัดการนำไฟฟ้าของโมลิบดีนัมไดซัลไฟด์พบว่าขณะที่ฉายแสงค่าการนำไฟฟ้ามีค่าเพิ่มขึ้นซึ่งสนับสนุนสมมติฐานที่ว่า การขยับของแถบวาเลนซ์ขณะที่ฉายแสงเป็นผลมาจากการที่อิเล็กตรอนถูกกระตุ้นให้ไปอยู่ที่แถบนำไฟฟ้า

สาขาวิชาฟิสิกส์  
ปีการศึกษา 2562

ลายมือชื่อนักศึกษา   
ลายมือชื่ออาจารย์ที่ปรึกษา 

PAKWAN CHANPRAKHON : ELECTRONIC STRUCTURE OF  
OPTICALLY EXCITED MOLYBDENUM DISULFIDE SINGLE  
CRYSTALS. THESIS ADVISOR : ASSOC. PROF. WORAWAT  
MEEVASANA, Ph.D. 54 PP.

MoS<sub>2</sub>/OPTICAL EXCITATION/ELECTRON DONATION/LASER IRRADIATION

Molybdenum disulfide (MoS<sub>2</sub>) is a famous material that has been studied to use in the electronic device because of its interesting electronic properties, which relate to its electronic structure. Angle-resolved Photoemission Spectroscopy (ARPES) is a powerful technique that has been used to directly measure the electronic structure of materials. In this work, the electronic structure variation of MoS<sub>2</sub> under laser irradiation in the fresh and doped (by potassium) MoS<sub>2</sub> samples were studied by using ARPES. For the freshly cleave MoS<sub>2</sub> sample, the shift of valence band to higher binding energy was observed during laser irradiation. This behavior is a result of the electrons being pumped into the conduction band by optical excitation. For the doped MoS<sub>2</sub> sample, we found that the shift of valence band to higher binding energy when compared to the valence band of fresh MoS<sub>2</sub> sample. This can be described by the donation of the electron from potassium to MoS<sub>2</sub> which corresponds with the presence of conduction pocket. By irradiated the laser to the doped sample, the shift of valence band to higher binding was also observed, which indicates that the electrons were also pumped to the conduction band in the doped sample. All of these behaviors of valence band shifts can be explained by the model of band diagram with the different located Fermi levels. These locations related to the Fermi level shifts due to laser irradiation and potassium

evaporation. According to conductance measurement, the increase of MoS<sub>2</sub> conductance under laser irradiation supports the explanation that the electrons are temporarily pumped from valence band to conduction band during laser irradiation.


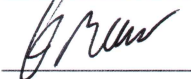


School of Physics

Academic Year 2019

Student's Signature

Advisor's Signature

## ACKNOWLEDGMENTS

My thesis could not be accomplished without supports from many people. First of all, I would like to thank my thesis advisor, Assoc. Prof. Dr. Worawat Meevasana. When I was an undergraduate student, I studied classical mechanics with him. I could not do my homework and I asked him for help. He calmly taught me that even though I was hard to understand. This made me very impressed with him. After that I have a chance to talk with him about the research, and it has been almost 5 years that I joined his research group. It is a very precious time for me. He gave me a big chance to perform the experiment in the USA, which is my valuable experience. He is very kind and nice advisor. I am very appreciated to him for his assistance in supervising and giving guidance with knowledge towards the resolution of this thesis.

I would like to acknowledge Asst. Prof. Dr. Panomsak Meemon, Assoc. Prof. Dr. Prayoon Songsiriritthigul and Dr. Hideki Nakajima for giving their valuable time to be the thesis defense committee and giving good suggestions for my work.

I am very thankful to everyone in Beamline 3.2a at Synchrotron Light Research Institute (SLRI) for helping me to perform the PES experiments.

I am fortunate to meet every member of Meevasana group. I would like to thank Dr. Tanachat Eknapakul for his big support and teaching me in many things. Without him, this work would not be done. I would like to thank Mr. Siwat Polin, Mr. Worasarit Saengsui, Miss Aissara Rasritat, Mr. Warakorn Jindata, Mr. Sujinda Chaiyachad and Mr. Suwat Thila for assisting me throughout the experiment. And I would like to thank

all of the members of Meevasana group for their help, kindness, entertainment and valuable friendship.

I am very thankful all teachers, all staffs and students in School of Physics, Institute of Science, Suranaree University of Technology for their supports.

I would like to acknowledge the Development and Promotion of Science and Technology Talents Project (DPST) scholarship for financial support since I was in a bachelor's degree.

I would like to thank my family and my friends. Firstly, I would like to deeply grateful to my parents who always give me a big love and significant support. Every day that I call with them, I feel like charging energy. I would like to thank my grandma who encourages me. Every time I feel discouraged, I call her, she always says to me that “my grandchild can do it”. That is very big energy for me. I would like to thank my sister who makes me feel relaxed when I am uneasy. I would like to thank my friends, Nut and Kad, for always listening to me. And finally, I am very thankful to all of my family and my friends. I would not have been achieved without their love, help and supports.

Pakwan Chanprakhon



# CONTENTS

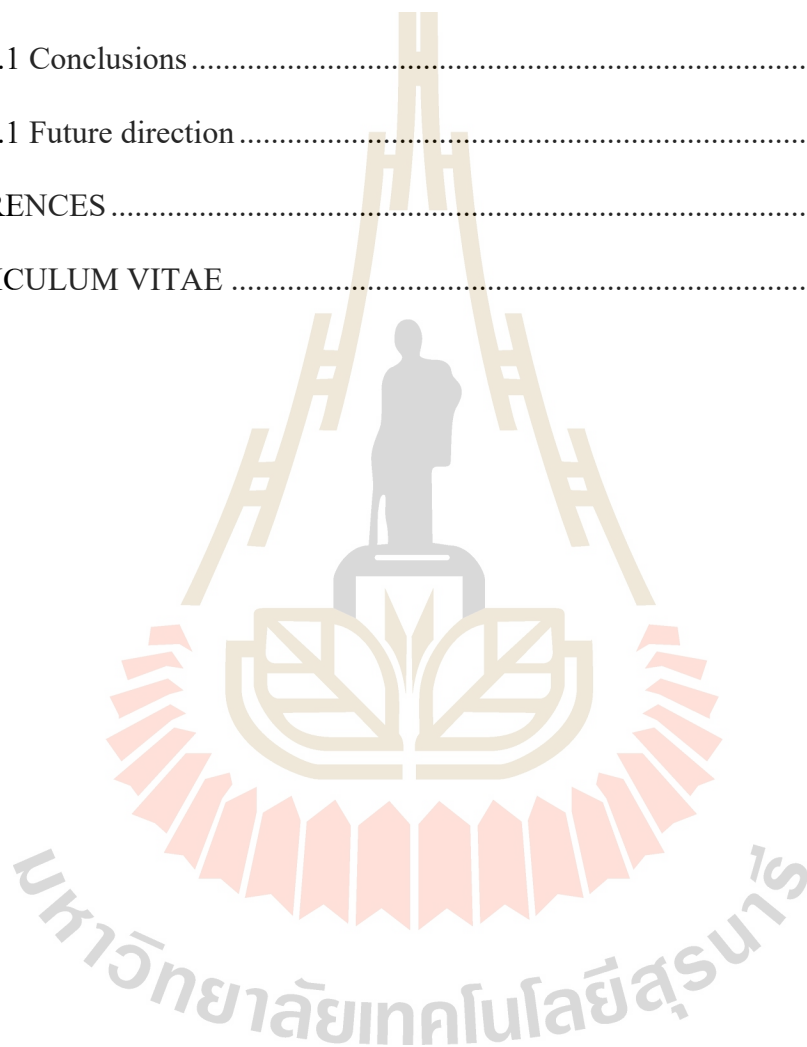
	<b>Page</b>
ABSTRACT IN THAI .....	I
ABSTRACT IN ENGLISH .....	II
ACKNOWLEDGMENTS .....	IV
CONTENTS .....	VI
LIST OF FIGURES .....	IX
<b>CHAPTER</b>	
<b>I INTRODUCTION .....</b>	<b>1</b>
1.1 Background and motivation .....	1
1.2 Objectives of research .....	5
1.3 Outline of thesis .....	6
<b>II LITERATURE REVIEWS &amp; THEORETICAL ASPECTS .....</b>	<b>7</b>
2.1 Literature reviews .....	7
2.1.1 Interesting optical properties of MoS <sub>2</sub> .....	7
2.1.2 Effect of light irradiation on the electronic structure .....	9
2.1.3 Effect of alkali metal evaporation in MoS <sub>2</sub> .....	12
2.2 Theoretical aspects .....	13
2.2.1 Reciprocal lattice .....	13
2.2.2 Fermi surface and Charge carrier density .....	15
2.2.3 Light Interaction in semiconductor .....	17

## CONTENTS (Continued)

	<b>Page</b>
2.2.4 Extrinsic semiconductor.....	20
<b>III METHODS .....</b>	<b>22</b>
3.1 Electronic Structure measured by Angle-resolved Photoemission Spectroscopy (ARPES).....	22
3.1.1 Photoemission spectroscopy (PES).....	22
3.1.2 Angle-resolved photoemission spectroscopy (ARPES).....	23
3.1.3 Photoemission process .....	25
3.1.4 Operation at Synchrotron Light Research Institute (SLRI), Thailand.....	29
3.2 Conductance measurement by 4-wire sensing .....	31
3.2.1 Principle of 4-wire sensing .....	31
3.2.2 Set up of the conductance measurement .....	32
<b>IV RESULTS AND DISCUSSION .....</b>	<b>34</b>
4.1 Electronic structure of MoS <sub>2</sub> by ARPES .....	34
4.1.1 Shift of valence band under laser irradiation in MoS <sub>2</sub> fresh sample.....	35
4.1.2 Doped MoS <sub>2</sub> sample by potassium evaporation .....	38
4.1.3 The model of MoS <sub>2</sub> band structure with different located Fermi levels .....	41
4.2 The increase of conductance measurement results .....	43

**CONTENTS (Continued)**

	<b>Page</b>
<b>V CONCLUSIONS .....</b>	<b>45</b>
5.1 Conclusions .....	45
5.1 Future direction .....	46
<b>REFERENCES .....</b>	<b>47</b>
<b>CURRICULUM VITAE .....</b>	<b>54</b>



## LIST OF FIGURES

Figure	Page
1.1 (a) monolayer TMD structure where transition metal and chalcogen atoms are black and yellow, respectively. (b) hexagonal TMDs structure from the top view .....	2
1.2 The increase of bandgap which related to the transition from indirect to direct band gap in MoS <sub>2</sub> .....	3
1.3 The emergence of conduction pocket at K(K') and the intercalation of potassium to the MoS <sub>2</sub> layer .....	4
1.4 The changing of current under UV irradiation.....	5
2.1 Schematic 3D view of single-layer transistor with hexagonal structure MoS <sub>2</sub> nanosheet, 50 nm-thick Al <sub>2</sub> O <sub>3</sub> dielectric, and ITO top-gate under monochromatic light .....	8
2.2 The switching between bright, neutral, and dark state of the TMDs heterostructure.....	8
2.3 Schematic of the electronic band structure for Bi <sub>2</sub> Se <sub>3</sub> . (a) Grey, shaded regions represent the bulk valence band (BVB) and bulk conduction band (BCB). Lines represent the SS with spin texture indicated. (b) The time-resolved-ARPES spectra of Bi <sub>2</sub> Se <sub>3</sub> near the $\Gamma$ point, the Bulk conduction band before the excitation (c) The bulk conduction band after optical excitation (d) Initial optical transition to high-lying bulk state (e) The SS	

## LIST OF FIGURES (Continued)

Figure	Page
<p>and BCB are populated by scattering from higher-lying states. (f) Energy relaxation of the SS and BCB populations are mostly completed. (g) A metastable population in the BCB .....</p>	10
<p>2.4 Variation of 2DEG charge density with exposure to different UV irradiation doses. (a)-(e), (g), and (h) show ARPES data for different irradiation doses .....</p>	11
<p>2.5 The measured resistance of the SrTiO<sub>3</sub> surface where the on-off process of the UV irradiation is as indicated. The inset shows the schematic diagram of the measurement setup.....</p>	11
<p>2.6 (a), (b) Valence band measured along the <math>\Gamma\text{-}\bar{K}</math> direction for bulk and monolayer MoS<sub>2</sub>, and (c) conduction band of monolayer MoS<sub>2</sub> .....</p>	12
<p>2.7 The experimental band structure of MoS<sub>2</sub> along the high symmetry lines. The panels (a) and (c) are for clean MoS<sub>2</sub>, while (b) and (d) following Na exposure to MoS<sub>2</sub> .....</p>	13
<p>2.8 (a) The unit cell with primitive vectors, <math>\vec{a}_1</math>, <math>\vec{a}_2</math>, and <math>\vec{a}_3</math> and angle <math>\alpha</math>, <math>\beta</math>, and <math>\gamma</math>. (b) The plane that has Miller indices (110) .....</p>	14
<p>2.9 Fermi level and Fermi momentum with the occupied and unoccupied state .....</p>	16

## LIST OF FIGURES (Continued)

Figure	Page
2.10 The transition of an electron in the same band (intraband transition) (b) The transition of an electron in the different bands (interband transition) .....	19
2.11 The generating of the electron-hole pair and the exciton by light. ....	20
3.1 Schematic diagram of Photoemission Spectroscopy technique. ....	23
3.2 The schematic diagram of APRES system, consisting of incident photon light, sample, and analyzer.....	24
3.3 Thee-step model and One-step model of photoemission process .....	26
3.4 MoS <sub>2</sub> sample preparation for ARPES measurement shows that the silver epoxy stuck between the sample holder, MoS <sub>2</sub> , and ceramic top post.....	30
3.5 Schematic diagram of resistance measuring circuit of (a) 2-wire system when the resistance of the sample is very high (b) 2-wire system when the resistance of the sample closes to the resistance of the wires. (c) 4-wire resistance measuring circuit .....	32
3.6 Schematic diagram of 4-wire conductance measuring setup .....	33
3.7 (Left) The MoS <sub>2</sub> sample and conductance measurement setup. (Right) The conductance measurement during laser irradiation.....	33
4.1 (a) The hexagonal Brillouin zone of MoS <sub>2</sub> which consist of 3 high symmetry point, $\Gamma$ , K and M. (b) The valence band of MoS <sub>2</sub> at $\Gamma$ point that was measured from ARPES .....	35

## LIST OF FIGURES (Continued)

Figure	Page
4.2 (a, b) The electronic band structure near the $\Gamma$ point of MoS <sub>2</sub> and irradiated sample, respectively. (c, d) The comparison of the magnified valence band at $\Gamma$ point of fresh and irradiated samples. ....	36
4.3 (a) MoS <sub>2</sub> electronic structure, red rectangle indicates the region using to calculate the EDCs. (b) The extracted EDCs near the $\Gamma$ point of MoS <sub>2</sub> between laser off and on .....	37
4.4 The valence band near the $\Gamma$ point of MoS <sub>2</sub> when the laser was switched between off and on .....	37
4.5 The comparison of valence band at $\Gamma$ point between fresh (a) and doped sample (b). (c) The comparison of EDCs between fresh and doped sample .....	39
4.6 The emergence of electron pocket at conduction band of the doped MoS <sub>2</sub> sample .....	39
4.7 The comparison of valence band at $\Gamma$ point between doped (a), doped-with-irradiation sample (b). (c) The comparison of EDCs between doped and doped-with-irradiation sample. ....	40
4.8 The comparison of all EDCs between fresh, fresh-with-irradiation, doped and doped-with-irradiation MoS <sub>2</sub> sample .....	40

## LIST OF FIGURES (Continued)

Figure	Page
4.9 The model of MoS <sub>2</sub> band structure with different located Fermi levels. The cyan curve represents the calculated MoS <sub>2</sub> band structure (from Eknapakul et al., 2014). The Fermi level positions of fresh, fresh-with-irradiation, doped and doped-with-irradiation sample were assumed to locate at E <sub>F1</sub> to E <sub>F4</sub> , respectively. ....	42
4.10 The $n_{2D}$ estimated from calculated band structure (cyan curve). The Fermi levels of fresh, fresh-with-irradiation, doped and doped-with-irradiation sample are highlighted with blue, red, green, and yellow, respectively .....	43
4.11 The switching of MoS <sub>2</sub> conductance as a function of various color laser irradiations every 10 seconds .....	44



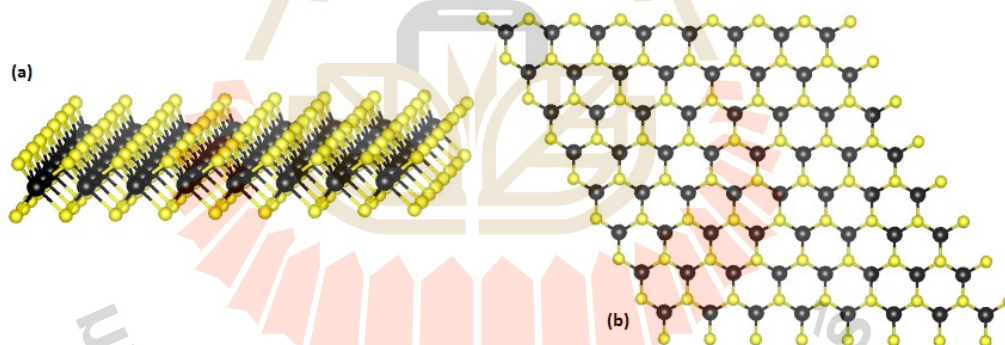
# CHAPTER I

## INTRODUCTION

### 1.1 Background and motivation

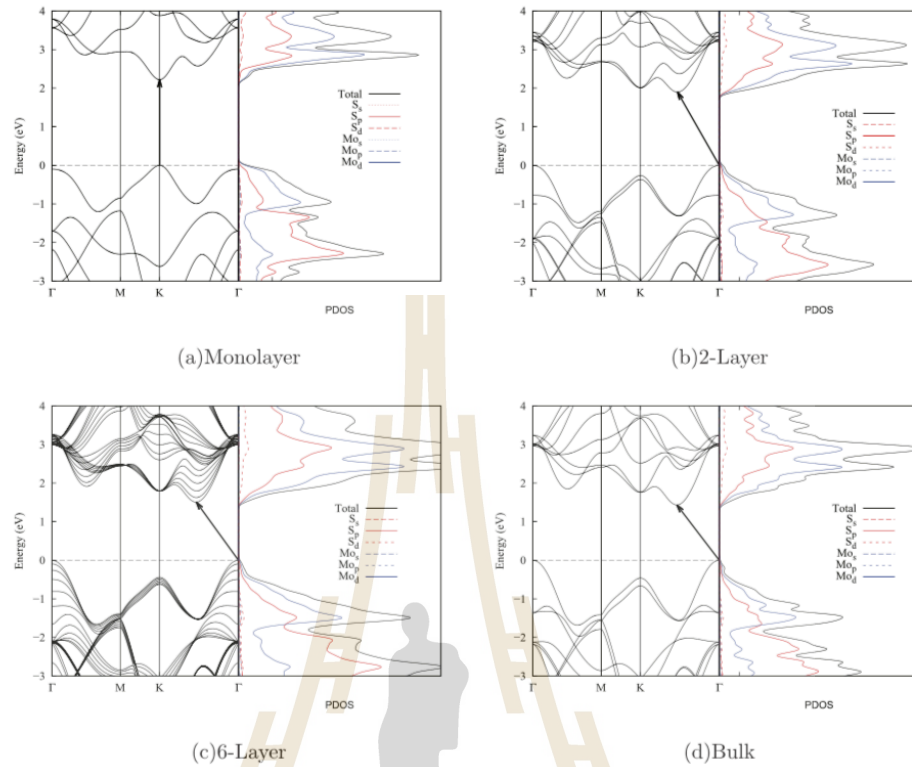
Graphene, the first example of two-dimensional materials discovered in 2004 (Novoselov et al., 2004), has been widely studied because of its excellent properties such as exceptional high mobility (Novoselov et al., 2004) and transparent conductor (Nair et al., 2008). From these interesting properties, graphene has been expected to be used in electronic devices such as sensors (Nag et al., 2017), energy storage (Pumera, 2010), and solar cells (Yin et al., 2013). After the discovery of graphene, many researchers have found other two-dimensional materials known as materials beyond graphene, such as semiconducting-transition metal dichalcogenides (TMDs). The few layers of graphene and TMDs can be easily produced by exfoliating (Bertolazzi et al., 2011; Li et al., 2014; Mak et al., 2010; Conley et al., 2013; Kang et al., 2018). TMDs are the layer materials consisting of the hexagonal lattice similar to graphene. As shown in Figure 1.1, monolayer TMDs form as the layer of transition metal atom (black) sandwich between the layer of the chalcogen atom (yellow) which is bond by ionic bonding. For the bulk TMDs, the monolayers of TMDs are bound together by weak van der Waals force like graphite. From previous studies, it was found that TMDs not only have high mobility but also possess the unique properties which have been expected to replace the silicon-based semiconductors (Bhimanapati et al., 2015; Mattheiss, 1973). The existence of their interesting physical and optical properties is capable of being

used in nanoelectronics and optoelectronics (Choi et al., 2017; Yun et al., 2012). Among more than 80 TMD compounds, MoS<sub>2</sub> is one of TMD materials that has been widely studied because it is robust and stable in the air. Interestingly, the modulation of their electronic properties, such as the crossover from indirect to direct band gap, can be observed when it was thinned down from multilayer to monolayer (Figure 1.2). Moreover, it was found that the optical properties of MoS<sub>2</sub> are strongly related to its electronic properties. For example, the enhanced photoluminescent intensity observed in MoS<sub>2</sub> monolayer which consistent with the transition of indirect to direct band gap (Splendiani et al., 2010; Eda et al., 2011). Furthermore, these behaviors are applicable in such tunable optical platforms including phototransistors (Lee et al., 2012; Yin et al., 2011), and photodetector (Lopez-Sanchez et al., 2013).



**Figure 1.1** (a) monolayer TMD structure where transition metal and chalcogen atoms are black and yellow, respectively. (b) hexagonal TMDs structure from the top view.

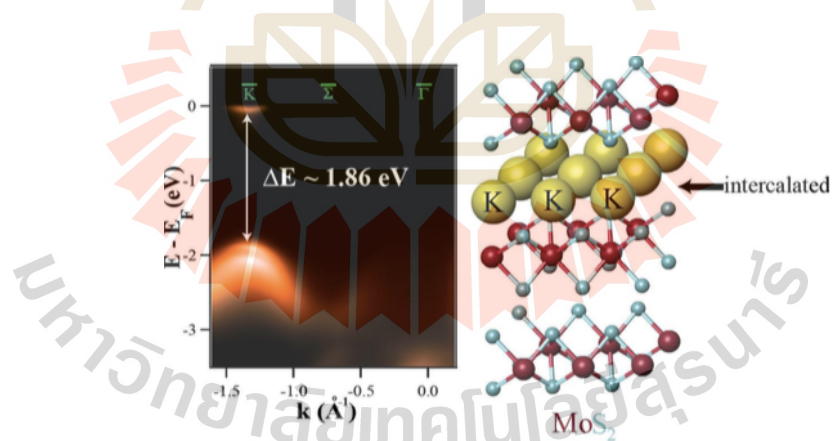
([https://en.wikipedia.org/wiki/Transition\\_metal\\_dichalcogenide\\_monolayers#/media/File:Monolayer\\_TMDC\\_structure.jpg](https://en.wikipedia.org/wiki/Transition_metal_dichalcogenide_monolayers#/media/File:Monolayer_TMDC_structure.jpg))



**Figure 1.2** The increase of bandgap which related to the transition from indirect to direct band gap in MoS<sub>2</sub>. (Ellis et al., 2011)

From the interesting properties that are related to their electronic structure, the electronic structure of materials can be probed by using angle-resolved photoemission spectroscopy (ARPES) (Coehoorn et al., 1987; Jin et al., 2013; Damascelli et al., 2004). The electronic structure variations by an external stimulus such as light irradiation and surface doping can also be observed by using ARPES. For example, by using time-resolved ARPES on the topological insulator Bi<sub>2</sub>Se<sub>3</sub>, the population of electrons in the surface and bulk conduction states of Bi<sub>2</sub>Se<sub>3</sub> were observed by pulse laser irradiation. This behavior indicated that the rich electrons can be excited by optical excitation (Sobata et al., 2012). Moreover, the effect of light irradiation has also been studied in several metal oxides (i. e. SrTiO<sub>3</sub>, KTO<sub>3</sub>) by ARPES. They suggest that the carrier

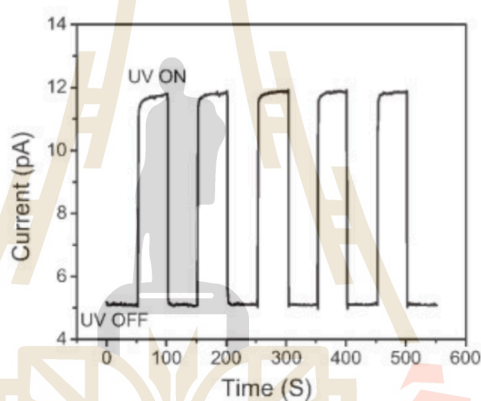
densities at the surfaces of these materials can be created and controlled through ultraviolet irradiation (Meevasana et al., 2011; King et al., 2012). In addition, the effect of alkali metal doping in TMDs with emerging properties has been studied by ARPES. For example, the quasi-freestanding monolayer MoS<sub>2</sub> can be created by potassium intercalation. As seen in Figure 1.3, the ARPES result shows the existence of conduction pocket at K(K') points which is a result of electron donation from alkali metal. The emergence of these conduction pockets is consistent with the electronic structure of MoS<sub>2</sub> monolayer which is caused by the intercalation of potassium atoms to the bulk MoS<sub>2</sub> (Eknapakul et al., 2014). Moreover, the negative electron compressibility and tunable spin splitting (Riley et al., 2015), Holstein polaron (Kang et al., 2018), and superconductivity (Zhang et al., 2016) have also been found in doped-TMDs by alkali metal.



**Figure 1.3** The emergence of conduction pocket at K(K') and the intercalation of potassium to the MoS<sub>2</sub> layer (Eknapakul et al., 2014).

Another one interesting effect of light in a semiconductor material is the changing of conductance. In a semiconductor, its conductance will be increased when

the light is shined into the sample as shown in Figure 1.4 (Fang et al., 2009). This property of semiconductors can be used in a light sensor (Hullavarad et al., 2009). Furthermore, the increase of the conductance under UV irradiation in SrTiO<sub>2</sub> was studied which is caused by the UV inducing the oxygen vacancies at its surface. The inducing of oxygen vacancies related to the creation of 2DEG states which are consistent with the ARPES result of the work that was mentioned before (Suwanwong et al., 2015).



**Figure 1.4** The changing of current under UV irradiation (Fang et al., 2008).

In this work, the electronic structure variation of bulk MoS<sub>2</sub> under light irradiation and potassium evaporation were studied by using ARPES. The variation of MoS<sub>2</sub> conductance under light irradiation has been measured by 4-wire sensing. The model of MoS<sub>2</sub> band structure with different located Fermi levels is used to describe overall results.

## 1.2 Objectives of research

- 1) To study the variation of electronic band structure of MoS<sub>2</sub> under laser

irradiation by ARPES.

2) To study the effect of potassium evaporation at the MoS<sub>2</sub> surface by ARPES.

3) To study the change of electrical conductivity of MoS<sub>2</sub> under laser irradiation.

4) To understand the mechanism that drives the change of MoS<sub>2</sub> band structure upon laser irradiation and potassium evaporation.

5) To understand the relationship between electronic structure and electrical conductivity of MoS<sub>2</sub> upon laser irradiation.

### 1.3 Outline of thesis

The thesis is separated into 5 chapters. Chapter I is the introduction part which includes the background and motivation, the two-dimensional materials, and their interesting properties. Chapter II presents the literature review and relating theoretical aspects. For the literature review, we explain the interesting optical properties of MoS<sub>2</sub>, the study of the effect of light in matter, and the effect of alkali metal evaporation at the surface of MoS<sub>2</sub> by ARPES. For the relating theoretical aspect, we demonstrate the reciprocal space, the Fermi surface and charge carrier density, the interaction of light in matter, and the extrinsic semiconductor. Chapter III discussed the principle of APRES and 4-wire sensing as well as the explanation of sample preparation and experimental setup. In chapter IV, the effect of laser irradiation and potassium evaporation at the surface of MoS<sub>2</sub> will be discussed. The study of MoS<sub>2</sub> conductance during laser irradiation and the model of MoS<sub>2</sub> band diagram with different located Fermi levels used to explain overall mechanisms will be described in this chapter. Chapter V includes the conclusion and future direction.

## CHAPTER II

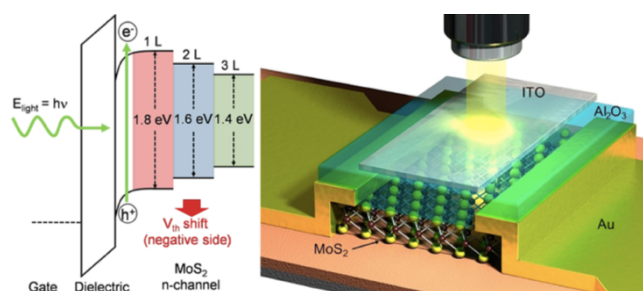
### LITERATURE REVIEWS & THEORETICAL ASPECTS

This chapter will be separated into two parts. The first part is a literature review of the interesting optical properties in MoS<sub>2</sub>, the effect of light irradiation on the electronic structure in matter, and the effect of alkali metal evaporation in MoS<sub>2</sub>. The second part will explain the relating theoretical aspects which consist of the relationship between real and reciprocal space lattice systems, the Fermi surface and charge carrier density, the electron excitation during light irradiation, and the effect of doping in semiconductor.

#### 2.1 Literature reviews

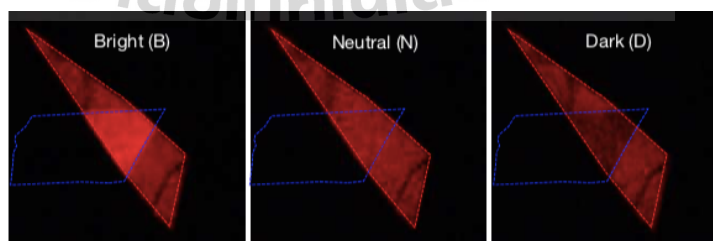
##### 2.1.1 Interesting optical properties of MoS<sub>2</sub>

MoS<sub>2</sub> is one of TMDs which possesses many interesting optical properties. In 2012, the tunable bandgap in the ultrathin MoS<sub>2</sub> based-phototransistor was studied as shown in Figure 2.1 (Lee et al., 2012). They reported the fabrication of the top gate phototransistor based-MoS<sub>2</sub> nanosheet. They found that the device consisting of the MoS<sub>2</sub> triple layer can detect the red color while the double and single layers responded to the green color. The different photo response has been described by the tunable band gap of MoS<sub>2</sub> by varying numbers of MoS<sub>2</sub> layers whose band gap is corresponded to 1.8, 1.65 and 1.35 eV for MoS<sub>2</sub> single, double and triple layers, respectively.



**Figure 2.1** Schematic 3D view of single-layer transistor with hexagonal structure MoS<sub>2</sub> nanosheet, 50 nm-thick Al<sub>2</sub>O<sub>3</sub> dielectric, and ITO top-gate under monochromatic light. (Lee et al., 2012)

Recently, the study of the blinking effect in the 2D TMDs based-heterostructure (i. e. MoS<sub>2</sub>, MoSe<sub>2</sub>, WS<sub>2</sub>, WSe<sub>2</sub>) was reported (Xu et al., 2017). This property has recently been reported to occur specifically in 0D or 1D materials (Nirmal et al., 1996; Dickson et al., 1997). They found that the blinking effect in TMDs heterostructure is different from those cases which exhibit only bright and dark states. In 2D TMDs heterostructure, this phenomenon randomly appears as bright, neutral, and dark states as shown in Figure 2.2. This behavior was explained by different charge transfer mechanisms between a gap of heterojunction as a result of different energy band alignment at heterojunctions, which corresponding to bright, neutral, and dark states.



**Figure 2.2** The switching between bright, neutral, and dark state of the TMDs heterostructures. (Xu et al., 2017)

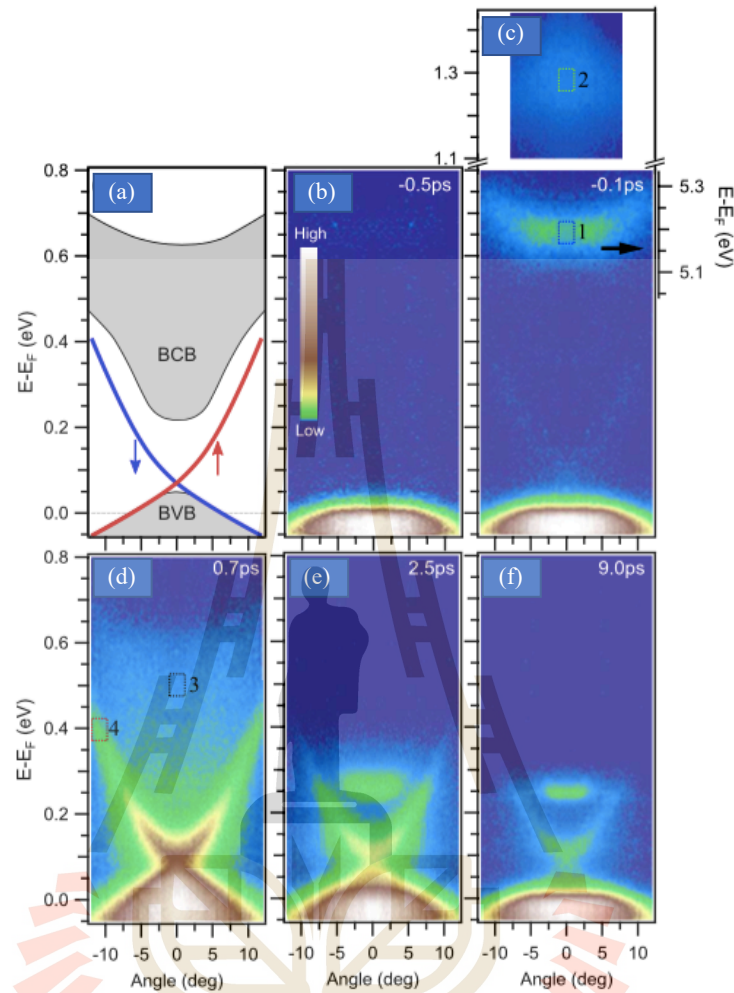


### 2.1.2 Effect of light irradiation on the electronic structure

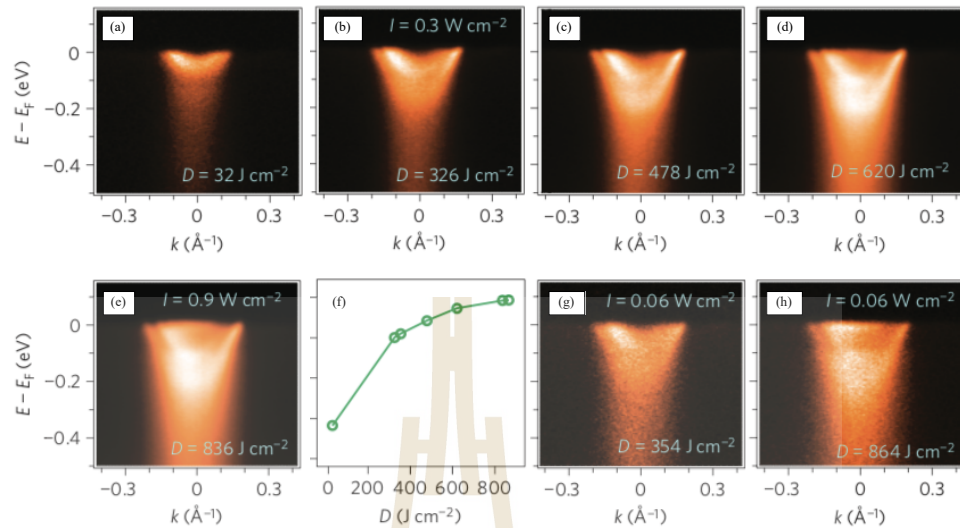
In 2012, the effect of optical excitation in the topological insulator  $\text{Bi}_2\text{Se}_3$  was studied by ARPES (Sobata et al., 2012). By using pulse-laser irradiation, as shown in Figure 2.3(c), it shows that electrons are excited to the high-lying state and then scattered to the bulk conduction band (BCB) and surface state (SS) (Figure 2.3(d)). After that, the electrons are gradually relaxed to SS and BCB. The increase of electron population in these states indicates that electrons are generated and donated to the CB upon optical excitation.

Furthermore, the effects of light irradiation have been studied in several metal oxides. In 2011, Meevasana et al. found that the two-dimensional electron gas (2DEG) state can be created at the bare surface of  $\text{SrTiO}_3$  by ultraviolet light irradiation (Meevasana et al., 2011). Figure 2.4 shows that the 2DEG density increases and the band move downwards upon increasing irradiation doses which suggest the control of 2DEG by UV irradiation. This behavior can also be observed in the surface  $\text{KTaO}_3$  (King et al., 2012).

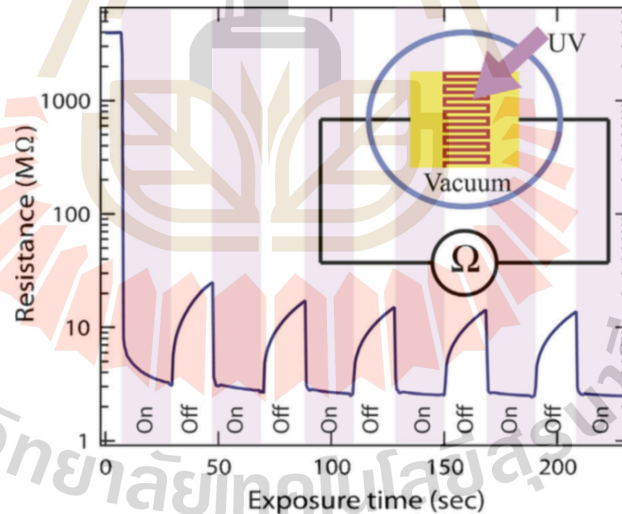
Suwanwong et al. further studied the effect of ultraviolet irradiation on the  $\text{SrTiO}_3$  single crystals (Suwanwong et al., 2015). They suggested that the 2DEGs induced by oxygen vacancies upon ultraviolet irradiation can be contributed to the changes in surface resistivity/conductivity. As seen in Figure 2.5, the modulation of  $\text{SrTiO}_3$  resistance can be found during light on/off which is related to the creation of the 2DEG state.



**Figure 2.3** Schematic of the electronic band structure for  $\text{Bi}_2\text{Se}_3$ . (a) Grey, shaded regions represent the bulk valence band (BVB) and bulk conduction band (BCB). Lines represent the SS with spin texture indicated. (b) The time-resolved-ARPES spectra of  $\text{Bi}_2\text{Se}_3$  near the  $\Gamma$  point, the Bulk conduction band before the excitation (c) The bulk conduction band after optical excitation (d) Initial optical transition to high-lying bulk state (e) The SS and BCB are populated by scattering from higher-lying states. (f) Energy relaxation of the SS and BCB populations are mostly completed. (g) A metastable population in the BCB. (Sobata et al., 2012)



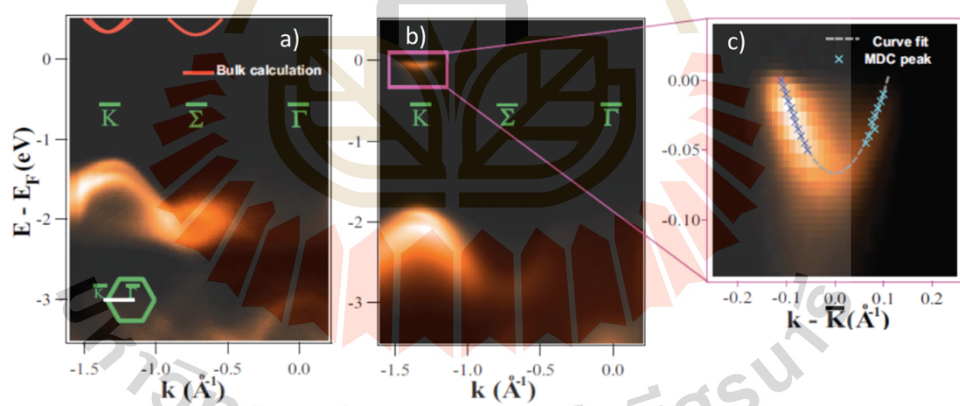
**Figure 2.4** Variation of 2DEG charge density with exposure to different UV irradiation doses. (a)-(e), (g), and (h) show ARPES data for different irradiation doses. (Meevasana et al., 2011)



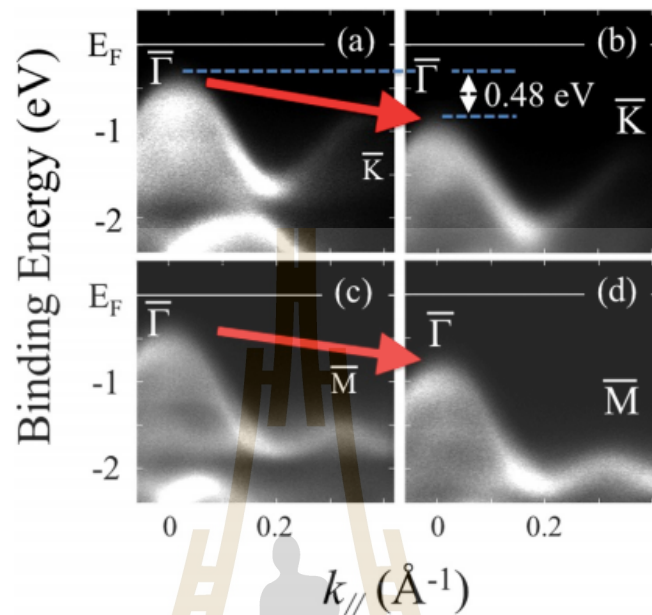
**Figure 2.5** The measured resistance of the SrTiO<sub>3</sub> surface where the on-off process of the UV irradiation is as indicated. The inset shows the schematic diagram of the measurement setup. (Suwanwong et al., 2015)

### 2.1.3 Effect of alkali metal evaporation in MoS<sub>2</sub>

Next, the electron donation achieved by alkali metal evaporation in MoS<sub>2</sub> has been studied. In 2014, Eknapakul et al. reported the effects of potassium evaporation in bulk MoS<sub>2</sub> by ARPES (Eknapakul et al., 2014). After the potassium evaporation, the ARPES results show that the valence band moves to higher binding energy as shown in Figure 2.6. This behavior can be described by the electron donation from potassium to MoS<sub>2</sub> which is consistent with the report from the efficient n-type doping by potassium deposition on a few-layer MoS<sub>2</sub> (Fang et al., 2013). In 2014, the effect of sodium evaporation on MoS<sub>2</sub> was also studied by ARPES (Komesu et al., 2014). They also found the shift of valence band of MoS<sub>2</sub> to higher binding energy is caused by the MoS<sub>2</sub> surface electron transfer as shown in Figure 2.7.



**Figure 2.6** (a), (b) Valence band measured along the  $\Gamma$ - $\bar{K}$  direction for bulk and monolayer MoS<sub>2</sub>, and (c) conduction band of monolayer MoS<sub>2</sub>. (Eknapakul et al., 2014)



**Figure 2.7** The experimental band structure of MoS<sub>2</sub> along the high symmetry lines. The panels (a) and (c) are for clean MoS<sub>2</sub>, while (b) and (d) following Na exposure to MoS<sub>2</sub>. (Komesu et al., 2014)

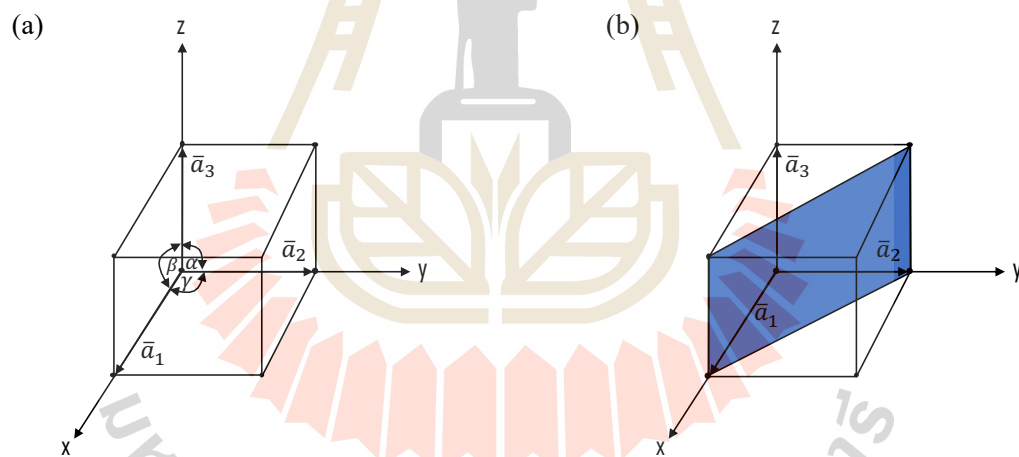
## 2.2 Theoretical aspects

### 2.2.1 Reciprocal lattice

The electronic structure of materials taken from ARPES was represented in the reciprocal space. Thus, the knowledge about the transition from real space to reciprocal space is required to understand the measured data. Lattice is an orderly set of points in a three-dimensional space in crystal. Obeying the fact that any points in the lattice will look the same. Lattice can be represented by three non-parallel primitive vectors ( $\vec{a}_1$ ,  $\vec{a}_2$  and  $\vec{a}_3$ ). The angles between those primitive vectors are written as  $\alpha$ ,  $\beta$ , and  $\gamma$  (Figure 2.8(a)). The translation between any two lattice points is demonstrated by the translation lattice vector (T)

$$\vec{T} = u_1 \vec{a}_1 + u_2 \vec{a}_2 + u_3 \vec{a}_3$$

where  $u_1$ ,  $u_2$  and  $u_3$  are integers. This means that moving the position in the lattice from one point to another point with the translation vector  $\vec{T}$ , the end point will be the same as the starting point. This is called ‘translation invariant’ which is the main property of the lattice system. The plane in real space lattice can be defined by using the Miller indices which are written as three integers in the bracket  $(hkl)$ . The numbers in the bracket  $(hkl)$  refer to the points that the plane cut along the x-, y-, and z-axis, respectively. For example, the (110) is the plane that is parallel to the z-axis and cut along x- and y-axis as shown in Figure 2.8(b). Note that the Miller indices are used to indicate the orientation of the sample.



**Figure 2.8** (a) The unit cell with primitive vectors,  $\vec{a}_1$ ,  $\vec{a}_2$  and  $\vec{a}_3$  and angle  $\alpha$ ,  $\beta$ , and  $\gamma$ . (b) The plane that has Miller indices (110).

In order to translate the real space to reciprocal space, the reciprocal lattice vector  $\vec{G}$  was defined which could be written as

$$\vec{G} = h\vec{b}_1 + k\vec{b}_2 + l\vec{b}_3$$

where  $hkl$  are Miller indices of the plane,  $\vec{b}_1$ ,  $\vec{b}_2$  and  $\vec{b}_3$  are primitive lattice vectors in reciprocal space.

Due to the periodic structure, the relation between real space lattice vector ( $\vec{R}$ ) and ( $\vec{G}$ ) follows this equation

$$e^{i\vec{G}\cdot\vec{R}} = 1$$

That implies  $\vec{G} \cdot \vec{R} = 2\pi N$  where  $N$  is integer and  $\vec{R}$  is equivalent to  $\vec{T}$ . The primitive lattice vector in reciprocal space ( $\vec{b}_1$ ,  $\vec{b}_2$  and  $\vec{b}_3$ ) can be written as following.

$$\vec{b}_1 = 2\pi \frac{\vec{a}_2 \times \vec{a}_3}{\vec{a}_1 \cdot (\vec{a}_2 \times \vec{a}_3)}$$

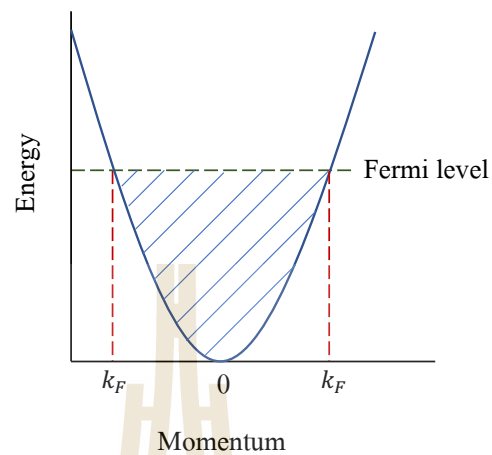
$$\vec{b}_2 = 2\pi \frac{\vec{a}_3 \times \vec{a}_1}{\vec{a}_2 \cdot (\vec{a}_3 \times \vec{a}_1)}$$

$$\vec{b}_3 = 2\pi \frac{\vec{a}_1 \times \vec{a}_2}{\vec{a}_3 \cdot (\vec{a}_1 \times \vec{a}_2)}$$

The reciprocal space can be used to explain the electronic structure of the materials which will describe in the next section.

### 2.2.2 Fermi surface and Charge carrier density

In this topic, we will explain the advantage of momentum space which has been used to calculate the charge carrier density. The Fermi surface and charge carrier density can be calculated from the electronic structure in momentum space. Figure 2.9 shows the energy level of the occupied and unoccupied state of the electron in momentum space. As seen in Figure 2.9, the momentum that the Fermi level cut the band was defined as Fermi momentum ( $k_F$ ).



**Figure 2.9** Fermi level and Fermi momentum with the occupied and unoccupied state.

The volume enclosed by the Fermi surface is defined as Luttinger volume which relates to the charge carrier density. If the Luttinger volume is equal to the volume of a Brillouin zone, it will be assumed that there are two electrons in a Brillouin zone because one energy band can be only two electrons. The decrease of Luttinger volume proportional to the electron density. Therefore, the electron density ( $n_{3D}$ ) which is the number of electrons per volume of the unit cell can be written as

$$n_{3D} = 2 \frac{V_{Luttinger}}{V_{k,cell}} \times \frac{1}{V_{R,cell}}$$

where  $V_{Luttinger}$  is the Luttinger volume.

$V_{k,cell}$  is the volume of the Brillouin zone.

$V_{R,cell}$  is the volume of the unit cell.



From the relation between  $V_{k,cell}$  and  $V_{R,cell}$ ,  $V_{k,cell} \cdot V_{R,cell} = (2\pi)^3 \cdot n_{3D}$  can be modified as

$$n_{3D} = 2 \frac{V_{Luttinger}}{(2\pi)^3}$$

For the 1D and 2D system, the charge carrier density can be written as

$$n_{2D} = 2 \frac{A_{Luttinger}}{(2\pi)^2}$$

And

$$n_{1D} = 2 \frac{L_{Luttinger}}{(2\pi)}$$

where  $A_{Luttinger}$  is the Luttinger area and  $L_{Luttinger}$  is the Luttinger length. The  $V_{Luttinger}$ ,  $A_{Luttinger}$  and  $L_{Luttinger}$  can be calculated from the Fermi momentum ( $k_F$ ).

### 2.2.3 Light Interaction in semiconductor

Electrons can be excited by the external sources of energy, i.e., laser, arc-discharge, or tungsten-halogen irradiation. Electron excitation is the phenomenon that electrons were excited from their ground states to the higher energy states by absorbing external energy matched with the energy separation between two levels. In atoms, the valence electron is the easiest electron which can be excited to the higher energy level. In solids, electrons in the valence band located near the Fermi level can be excited easier than the electrons in the deeper band, e.g. core level. In metals, no energy is required to excite electrons in metals because of their zero band gaps. For the insulators and semiconductors, the insulators require more energy than semiconductors to excite electrons because of their larger band gap (Paudel, 2014). The transition of electrons to higher energy can be separated by two mechanisms. The first one is the transition of

electrons at the same level, e.g. in the conduction band or valence band themselves. This process is called “intraband transition” which is shown in Figure 2.10(a). Another mechanism is the transition of an electron to a different energy level which is called “interband transition” (Figure 2.10(b)). Thus, we will consider the most possible transition.

From the conservation of energy,

$$\text{Final Energy} = \text{Initial Energy} + \text{Photon energy}$$

Let's consider the electron with the initial momentum  $\vec{k}_i$  and energy  $E_n(\vec{k}_i)$  which absorbs the photon energy  $\hbar\omega$  and transfers to a state with final momentum  $\vec{k}_f$  and energy  $E_m(\vec{k}_f)$ . The conservation of energy is then followed the equation

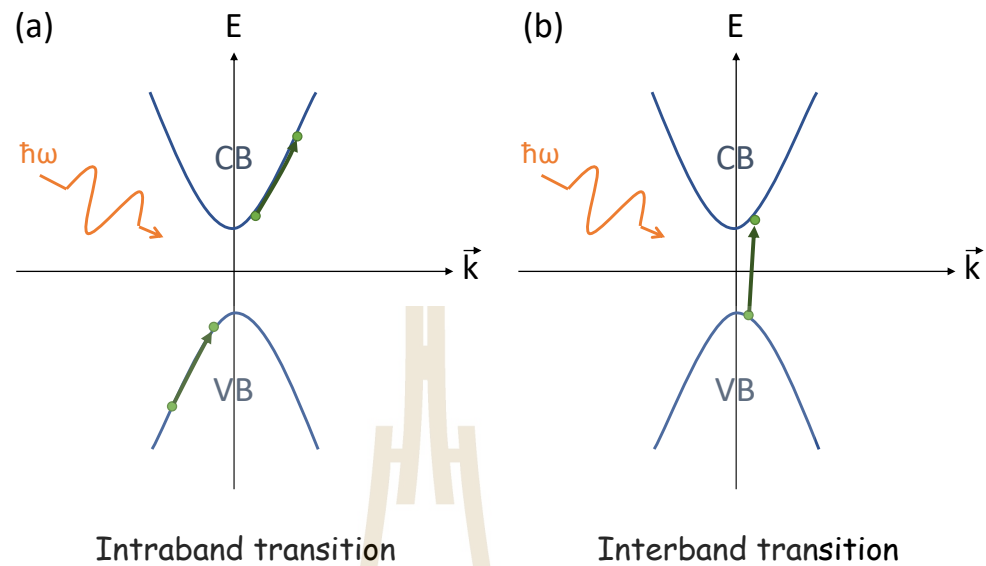
$$E_m(\vec{k}_f) = E_n(\vec{k}_i) + \hbar\omega$$

In addition to the conservation of energy rule, the momentum should be conserved as shown in the following equation

$$\vec{k}_f = \vec{k}_i + \vec{q}$$

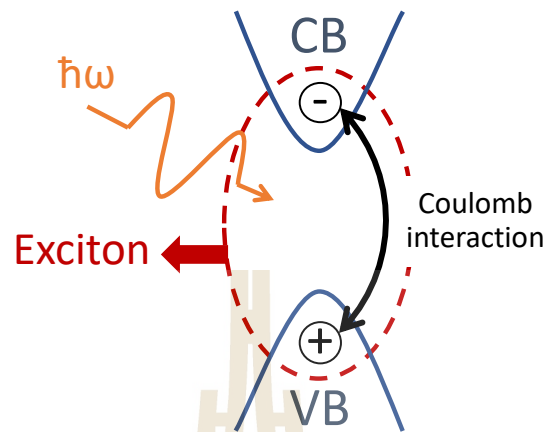
where  $\vec{q}$  is the momentum of the photon.

From the parabolic-like band dispersion, the intraband transition is not allowed because it cannot follow both conservation rules. The conservation of momentum is broken in the transition in the same band. Therefore, the interband transition is only allowed to occur which is the transition of electrons from initial to final state in the different bands (Rana, F.).



**Figure 2.10** (a) The transition of an electron in the same band (intraband transition) (b) The transition of an electron in the different bands (interband transition).

In semiconductors, when electrons absorb energy which is higher than their energy gap, the electrons will be excited to the conduction band. The empty state in the valence band is assigned as a positive charge particle which is called a “hole” with its own mass. The coupling between electron and hole was called “electron-hole pair”. The electron and hole could be bound due to the Coulomb interaction which is called “exciton” as shown in Figure 2.11. From the excitation of electrons, the conduction band was filled by the number of electrons, which is resulted in the increase of conductance in semiconductors. The changes of conductance induced by light have been widely used in optoelectronic devices such as photoresistors, phototransistors, and photodetectors.



**Figure 2.11** The generating of the electron-hole pair and the exciton by light.

#### 2.2.4 Extrinsic semiconductor

An extrinsic semiconductor is a conventional semiconductor that is doped by other atoms whereas the undoped semiconductor was called ‘intrinsic semiconductor’. Extrinsic semiconductors were established to modify their electrical properties which are widely used in nowadays electronic devices such as diodes and transistors. The extrinsic semiconductor can be separated into p- and n-type depending on their impurity dopant. For p-type semiconductors, the intrinsic semiconductors are doped by an electron acceptor element (e.g. Boron or Gallium in Silicon). The p-type semiconductors possess higher hole concentration than electron concentration. Thus, holes are major carriers while electrons are minor carriers in p-type semiconductors. On the other hand, n-type semiconductors can be created by doping an intrinsic semiconductor with an electron donor element (e.g. Phosphorus or Arsenic in Silicon). The donation of electrons from the dopants leads to higher electron density than holes density, therefore, electrons are major carriers in n-type semiconductors. In

doped semiconductors, the Fermi level ( $E_F$ ) or chemical potential can be shifted toward conduction or valence bands depending on dopants which is related to this following equation

$$E_F = \frac{E_c + E_v}{2} + kT \ln\left(\frac{n_D}{n_A}\right)$$

where  $E_c$  and  $E_v$  are the conduction band and valence band energy positions.  $n_D$  and  $n_A$  are the donor and acceptor density, respectively.

From the above equation, it is seen that the Fermi level of extrinsic semiconductors moves toward the conduction band in n-type semiconductors while moves toward valence band in p-type semiconductors. Hence, doping is a crucial parameter that can modify the electronic property of semiconductors.

## **CHAPTER III**

### **METHODOLOGY**

In this section, we will talk about the experiment which is separated into two main parts. The experiment consists of the measurement of MoS<sub>2</sub> electronic structure by ARPES and the conductance measurement by 4-wire sensing. In the first part, the principle of ARPES will be discussed which will be started with the photoelectric effect. The photoemission spectroscopy will be clarified in the topic of ARPES and Photoemission process. Furthermore, the sample preparation and ARPES experimental setup will be explained. In the second part, the principle of 4-wire sensing which is the development from 2-wire sensing to 4-wire sensing will be discussed with their advantage and disadvantage. Finally, the sample preparation and the setup of conductance measurement will be illustrated below.

#### **3.1 Electronic Structure measured by Angle-resolved Photoemission Spectroscopy (ARPES)**

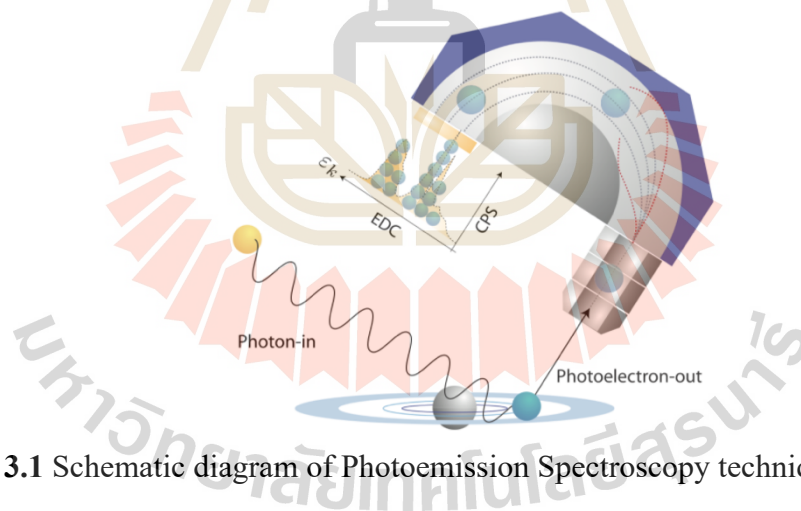
##### **3.1.1 Photoemission spectroscopy (PES)**

Photoemission spectroscopy (PES) is a direct and powerful technique to probe the electronic structure of the materials. The technique is based on the photoelectric effect. Firstly, Photoelectric effect is the phenomenon that was discovered by Heinrich Hertz in 1887. After that Albert Einstein can explain this phenomenon by using

Planck's idea that light can be a particle (called "photon"). In the photoelectric effect, the light or photon in which known energy is shined to the sample. If the energy of the photon is higher than the binding energy ( $E_B$ ) and the work function ( $\phi$ ), the electrons will be knocked out of the sample that are called "photoelectron". In photoemission spectroscopy, the kinetic energy ( $E_k$ ) of the electrons are measured by the detector as shown in Figure 3.1. And the kinetic energy of the photoelectron can be converted to the binding energy as the following equation

$$E_k = hf - E_B - \phi \quad (3.1)$$

Normally, the work function of the analyzer is higher than that of the sample. Hence, the work function for PES can be used the work function of the analyzer as the reference.



**Figure 3.1** Schematic diagram of Photoemission Spectroscopy technique.

([www.slri.or.th](http://www.slri.or.th))

### 3.1.2 Angle-resolved Photoemission Spectroscopy (ARPES)

For Angle-resolved Photoemission Spectroscopy (ARPES), the analyzer can measure the angle ( $\theta$ ) of the photoelectrons that were ejected from the surface of the

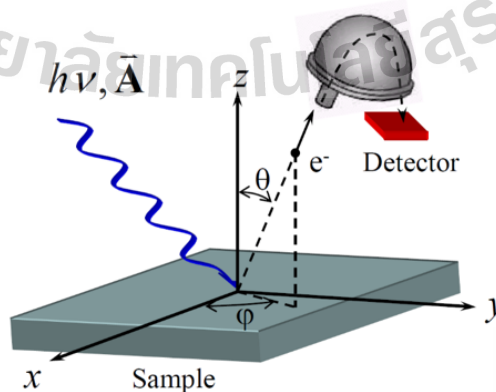
sample as shown in Figure 3.2. In crystal surface, in-plane momentum  $k_{//}$  is conserved because of the translation symmetry in the x-y plane. The  $k_{//}$  can be converted from the angle of the photoelectron ( $\theta$ ) as following the equation.

$$k_{//} = \sqrt{\frac{2m_e E_k}{\hbar^2}} \sin\theta \quad (3.2)$$

For the perpendicular plane momentum,  $k_{\perp}$  becomes more complicated because the surface potential ( $V_0$ ) appears in the equation.  $k_{\perp}$  is written as

$$k_{\perp} = \sqrt{\frac{2m_e(E_k+V_0)}{\hbar^2}} \cos\theta \quad (3.3)$$

When electrons travel through the sample surface interface,  $k_{\perp}$  is not conserved because of the lack of translation symmetry along the perpendicular surface. Thus,  $k_{\perp}$  cannot be directly measured from ARPES. In two-dimensional materials, the problem of  $k_{\perp}$  is not effective due to the no dispersion along the z-direction. The relation between the  $E_k$  and  $k_{//}$  from equation (3.1) and (3.2) are related to the electronic band structure. Therefore, we can get the electronic band structure of the materials from ARPES. And the rotation of the sample relates to the measurement of the band structure at other interesting points in the Brillouin zone.



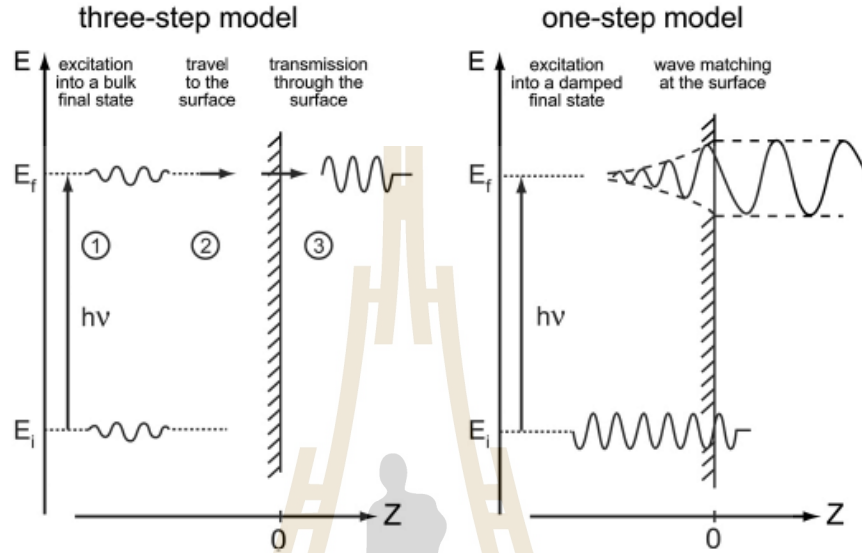
**Figure 3.2** The schematic diagram of APRES system, consisting of incident photon light, sample, and analyzer.



### 3.1.3 Photoemission Process

To understand more about the photoemission process, the behavior of electrons can be explained by using a three-step model and one-step model. The one-step model describes the whole photoemission process as one single step. As shown in Figure 3.3(right), when the electron absorbs the energy, the photoelectron was excited and formed the damp final state near the surface. The damping state of the electron takes care of the whole process traveling through the surface with a short mean free path. The surface excitation has to be considered the phase matching of the wavefunction at the surface. The complexity of this one-step model makes it difficult to calculate. Therefore, the three-step model has been widely used to explain photoemission. The three-step model explains the photoemission process by separating into 3 steps as shown in Figure 3.3 (left): (i) The excitation of the photoelectron inside the sample. This step explained the excitation of the electron from the initial state to the final state when the electron absorbs the photon energy and generates an electron-hole pair inside the crystal. The transition probability of the electron in the ground state to the possible final state was given by Fermi golden rule, which will be discussed later. (ii) The transport of photoelectron to the surface. This process described that the electrons travel to the surface without scattering in the crystal. It can be explained in the term of the probability proportional to an effective-mass-mean-free-path of the materials. In this process, if some electrons interact in-elastically to the system, they will give some inelastic electron which will add to the background spectra. This needless background is usually subtracted. (iii) The escape of photoelectron into the vacuum. The electrons will be escaped from the surface if their energy is higher than the work function of the

materials. In this process,  $k_{\perp}$  is changed depending on the excitation energy and the surface of the sample.



**Figure 3.3** Three-step model and One-step model of photoemission process. (Hüfner, 1995)

Here, we will consider the ARPES intensity which relates to transmission probability in the three-step model of the photoemission process. From the Fermi's golden rule, the transition probability of  $N$ -electron ground state into one possible final state by photoexcitation can be written as

$$\omega_{f,i} = \frac{2\pi}{\hbar} |\langle \psi_f^N | H_{int} | \psi_i^N \rangle|^2 (E_f^N - E_i^N - \hbar\nu) \quad (3.4)$$

where  $\psi_i^N$  and  $\psi_f^N$  are the initial state and final state energies of  $N$  particle system, respectively. The Hamiltonian of electron-photon interaction can be written as

$$H_{int} = -\frac{e}{2mc} (\mathbf{A} \cdot \mathbf{p} + \mathbf{p} \cdot \mathbf{A}) \quad (3.5)$$

Where  $\mathbf{p}$  and  $\mathbf{A}$  are the electronic momentum operator and electromagnetic vector potential, respectively. Assuming the photoemission process suddenly happened, the initial and final state can be written as

$$\psi_i^N = A\phi_i(k)\psi_i^{N-1} \quad (3.6)$$

$$\psi_f^N = A\phi_f(k)\psi_f^{N-1} \quad (3.7)$$

where  $A$  is the proper  $N$  electron wave function antisymmetric operator.  $\phi_i(k)$  and  $\phi_f(k)$  are the wave function of photoelectron in the initial state and final state, respectively.  $\psi_i^{N-1}$  is the wave function of the remaining  $(N-1)$  electrons and  $\psi_f^{N-1}$  is the wave function of the  $(N-1)$  electron left behind. The ARPES intensity is a summation over all states which can be written as

$$I(k, E_k) = \sum_{f,i} \omega_{f,i} = \sum_{f,i} \frac{2\pi}{\hbar} |\langle \psi_f^N | H_{int} | \psi_i^N \rangle|^2 \delta(E_f^N - E_i^N - h\nu) \quad (3.8)$$

Substitute  $\psi_i^N$  and  $\psi_f^N$  to  $\langle \psi_f^N | H_{int} | \psi_i^N \rangle$ , we will get

$$\langle \psi_f^N | H_{int} | \psi_i^N \rangle = M_{f,i}^k \langle \psi_s^{N-1} | \psi_i^{N-1} \rangle = M_{f,i}^k c_s \quad (3.9)$$

The  $\psi_f^{N-1}$  is replaced by eigenstate  $\psi_s^{N-1}$ . Thus, the total intensity is

$$I(k, E_k) = \sum_{f,i} |M_{f,i}^k|^2 \sum_s |c_s|^2 \delta(E_k + E_s^{N-1} - E_i^N - h\nu) \quad (3.10)$$

where  $|c_s|^2 = |\langle \psi_s^{N-1} | \psi_i^{N-1} \rangle|^2$  is the probability of the electron in the initial state  $i$  can be left to the final state  $s$ . In non-interacting system,  $\psi_i^{N-1} = \psi_{s_0}^{N-1}$ ,  $c_s$  become 1 for one particular state,  $s = s_0$ , and all other become zero. From this result, all peaks in the ARPES spectrum are formed as a delta function and have a zero width. On the contrary, in a strongly correlated system, many of  $|c_s|^2$  are not equal to zero due to the

overlapping of  $\psi_i^{N-1}$  with many eigenstate  $\psi_s^{N-1}$ . Therefore, the ARPES spectrum is not only the single delta function but it also consists of many delta functions related to the number of excited states. The ARPES intensity for a 2D single-band system can be written as

$$I(k, \omega) = I_0(k, \nu, \mathbf{A})f(\omega)A(k, \omega) \quad (3.11)$$

where  $k$  is the in-plane electron momentum.  $\omega$  is electron energy related to the Fermi level.  $\mathbf{A}$  is the polarization of the incoming photon. The term  $f(\omega)$  is the Fermi Dirac function which can be probed only occupied state. In 2D system,  $I_0(k, \nu, \mathbf{A})$ , which related to the matrix element  $|M_{f,i}^k|^2$ , is slowly varying. Thus, the photoemission can be directly probed the spectral function  $A(k, \omega)$  which comes from the Green's function formalism. The total spectral function can be written as

$$A(k, \omega) = -\frac{ImG(k, \omega)}{\pi} \quad (3.12)$$

The Green's function in this case can be represent as

$$G(k, \omega) = \frac{1}{\omega - \varepsilon_k - \Sigma(k, \omega)} \quad (3.13)$$

where  $\Sigma(k, \omega)$  is term of electron self-energy  $\Sigma(k, \omega) = \Sigma'(k, \omega) + i\Sigma''(k, \omega)$ .  $\Sigma'(k, \omega)$  and  $\Sigma''(k, \omega)$  are related to the renormalization of the bare band dispersion ( $\varepsilon_k$ ) and scattering rate, respectively. Substituted (3.13) to the spectral function (3.12), we will get the expression of spectral function as

$$A(k, \omega) = -\frac{1}{\pi} \frac{Im\Sigma(k, \omega)}{[\omega - \varepsilon_k - Re \Sigma(k, \omega)]^2 + [Im \Sigma(k, \omega)]^2} \quad (3.14)$$

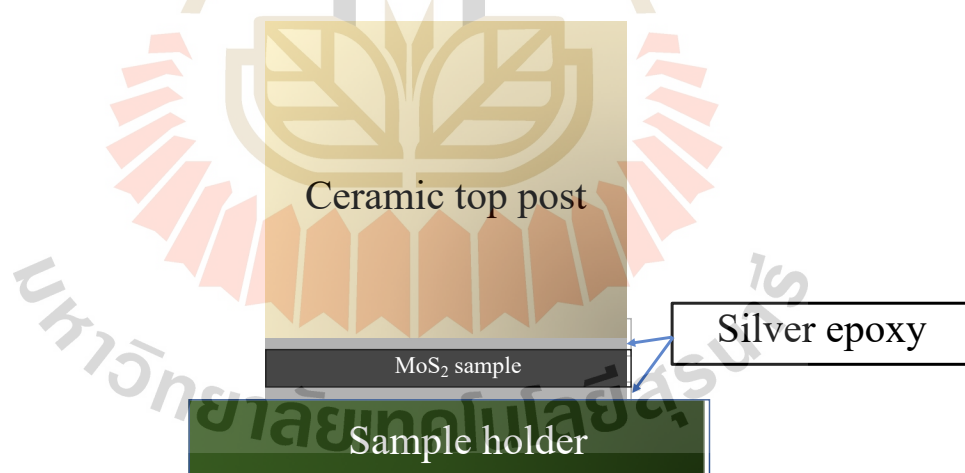
From this expression, the spectral function is given a form as a Lorentzian function. In general, the electron-electron correlation appears in many systems. Adding one electron to the system is related to the whole system. To make its simplification, the quasiparticle has been used to explain. The quasiparticle describes that correlated electrons are composed of virtual excitation and continuous movement with the electrons through the crystal. Therefore, in the correlated system, the spectral function can be expressed as the Lorentzian function related to the energy and lifetime of quasiparticle.

### **3.1.4 Operation at Synchrotron Light Research Institute (SLRI), Thailand**

ARPES results will be measured at Beamline 3.2a at SLRI using SCIENTA R4000 hemispherical analyzer. Preparation of the MoS<sub>2</sub> sample for ARPES measurement was shown in Figure 3.4, the bottom of the sample was attached to the holder by silver epoxy. The face of the sample was glued with the ceramic top post by silver epoxy, which is ready for cleaving the surface of the sample. For ARPES measurement, firstly, the sample was loaded to the load lock. When the pressure in the load lock under  $10^{-7}$  mbar, the sample was transferred to the manipulator in the preparation chamber. After that, the sample was cleaved in ultrahigh vacuum at pressure better than  $9 \times 10^{-9}$  mbar to provide a pristine surface. Then, the sample was measured in the main chamber under pressure better than  $10^{-9}$  mbar. Measurements were carried out using the photon energy 60 eV that were produced from the synchrotron light source. The temperature of the system was cooled down to 80 K. The laser with a wavelength of 450 nm (corresponding to 2.75 eV) was used as an irradiation source throughout the ARPES experiment.

### *Potassium Evaporation*

Potassium is the chemical element in group 1 alkali metal known as the material that is easy to donate electrons to the other material. The potassium depositions were achieved by biasing the SAES Getter evaporation source. The potassium source was equipped at the preparation chamber. Firstly, the potassium source was heated by biasing the current 3 A (increasing step by 0.2 A) for degassing the source. After that, the sample was moved to the preparation chamber and turned the sample face to the evaporating source. The current was increased to 5.5 A that higher than the boiling point of potassium. The increase of the pressure in the preparation chamber confirms that the potassium was transpired from potassium source and evaporated to the surface of the sample. The evaporated process was held at biasing current 5.5 A for 10 minutes.



**Figure 3.4** MoS<sub>2</sub> sample preparation for ARPES measurement shows that the silver epoxy stuck between the sample holder, MoS<sub>2</sub>, and ceramic top post.

## 3.2 Conductance measurement by 4-wire sensing.

### 3.2.1 Principle of 4-wire sensing

In this section, the principle of 4-wire resistance measurement will be explained. We will start with the development from 2-wire sensing to 4-wire sensing. Normally, 2-wire system has been widely used to measure the electrical conductance of the sample. It is suitable for the sample with high resistance, but it is inaccurate for the low resistance sample. For the resistance of the sample is very higher than that of the wire, we can ignore the resistance of the wires in the circuit as shown in Figure 3.5(a). The resistance of the sample is following the equation

$$R_{measure} = \frac{V_{measure}}{I} = R_{sample} \quad (3)$$

However, If the resistance of the sample is close to that of the wires, the resistance of the wire will affect the system. Thus, the resistance that was measured from the 2-wire system was following the equation

$$R_{measure} = \frac{V_{measure}}{I} = R_{sample} + 2R_{wire} \quad (4)$$

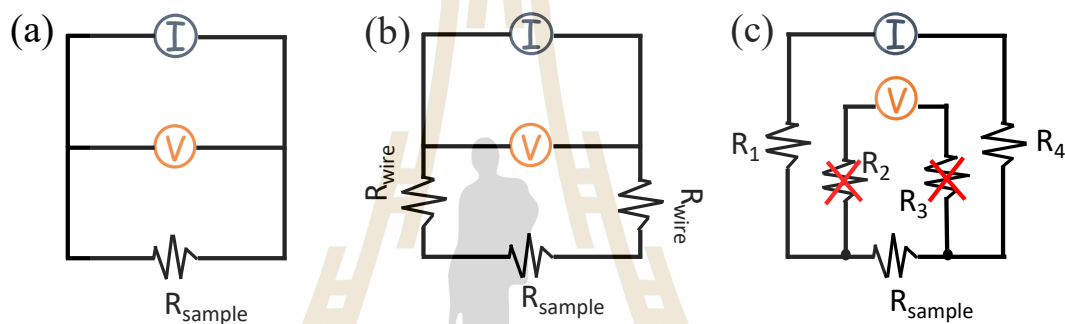
Nowadays, 4-wire sensing has been developed for measuring the resistance in the low resistance sample. 4-wire sensing is a technique to precisely measure the electrical conductance. The 4-wire resistance measuring is also known as Kelvin sensing. This technique was invented by Lord Kelvin and William Thomsom in 1861.

The system consists of 4 electrical wires, two wires are contacted to the voltmeter whereas another two wires are contacted to the current source as shown in Figure 3.5(c). From this setup, the current flow through the two outer connectors and generate the voltage across  $R_1$ ,  $R_4$ , and  $R_{sample}$ . Due to the voltmeter has a drastically high impedance, the current does not go through the  $R_2$  and  $R_3$ . The voltage measured from

the voltmeter was only the voltage across the sample. Thus, the  $R_{\text{sample}}$  can be calculated following the equation.

$$R_{\text{measure}} = \frac{V_{\text{measure}}}{I} = R_{\text{sample}} \quad (5)$$

Therefore, four-wire resistance measuring can be used to eliminate the resistance from the electrical wires to get the accurate resistance of the sample.



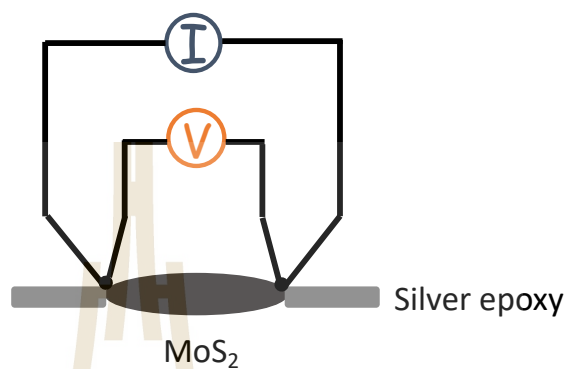
**Figure 3.5** Schematic diagram of resistance measuring circuit of (a) 2-wire system when the resistance of the sample is very high (b) 2-wire system when the resistance of the sample closes to the resistance of the wires. (c) 4-wire resistance measuring circuit.

### 3.2.2 Set up of the conductance measurement

In this work, the  $\text{MoS}_2$  conductance was measured by the 4-wire system. Figure 3.6 shows the schematic diagram of the 4-wire resistance measuring setup. For the sample preparation, the  $\text{MoS}_2$  with a diameter approximately of 0.5 mm were electrically contacted by using silver epoxy as shown in Figure 3.7(left). The  $\text{MoS}_2$  conductance was measured as a function laser source with energies of 2.75, 2.33, 1.9 eV, respectively, as shown in Figure 3.7(right). The conductance measurements were repeatedly performed during each laser on and off every 10 seconds for several cycles.



The laser sources were fixed with the 80 mW power. The conductance was calculated from the measured current at a fixed bias voltage of 10 V (e.g.  $C=I/V$ ).



**Figure 3.6** Schematic diagram of 4-wire conductance measuring setup.



**Figure 3.7** (Left) The MoS<sub>2</sub> sample and conductance measurement setup. (Right) The conductance measurement during laser irradiation.

## **CHAPTER IV**

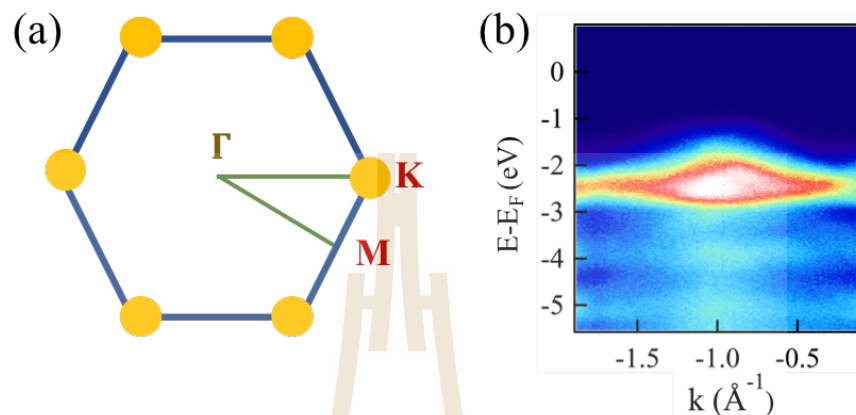
### **RESULTS AND DISCUSSION**

In this chapter, the results and discussion of this work will be explained. we will start with the MoS<sub>2</sub> band structure results that were measured from ARPES. Then, we will talk about the shift of MoS<sub>2</sub> band structure during laser irradiation. Furthermore, the doped MoS<sub>2</sub> by potassium evaporation was studied by ARPES and the shift of the doped MoS<sub>2</sub> by laser irradiation was also studied. We propose the model of MoS<sub>2</sub> band structure with different located Fermi levels to explain the change of MoS<sub>2</sub> electronic structure under laser irradiation and potassium evaporation. The conductance measurement under light irradiation measured by the 4-wire technique will also be demonstrated.

#### **4.1 Electronic structure of MoS<sub>2</sub> by ARPES**

MoS<sub>2</sub> is the two-dimensional material that has the hexagonal Brillouin zone which consists of 3 high symmetry interesting points ( $\Gamma$ , K, and M). As shown in Figure 4.1(a),  $\Gamma$ , K, and M are the points that locate at the center of the Brillouin zone, hexagon corner, and hexagon edge center, respectively. The electronic band structure of MoS<sub>2</sub> was carried out using ARPES located at Beamline 3.2a, SLRI. Figure 4.1(a) shows the ARPES result of the valence band maximum near the  $\Gamma$  point. This is consistent with previous experiments (Eknapakul et al., 2014). Further measurements including the

variation of MoS<sub>2</sub> valence band was studied as a function of laser irradiation and potassium evaporation.



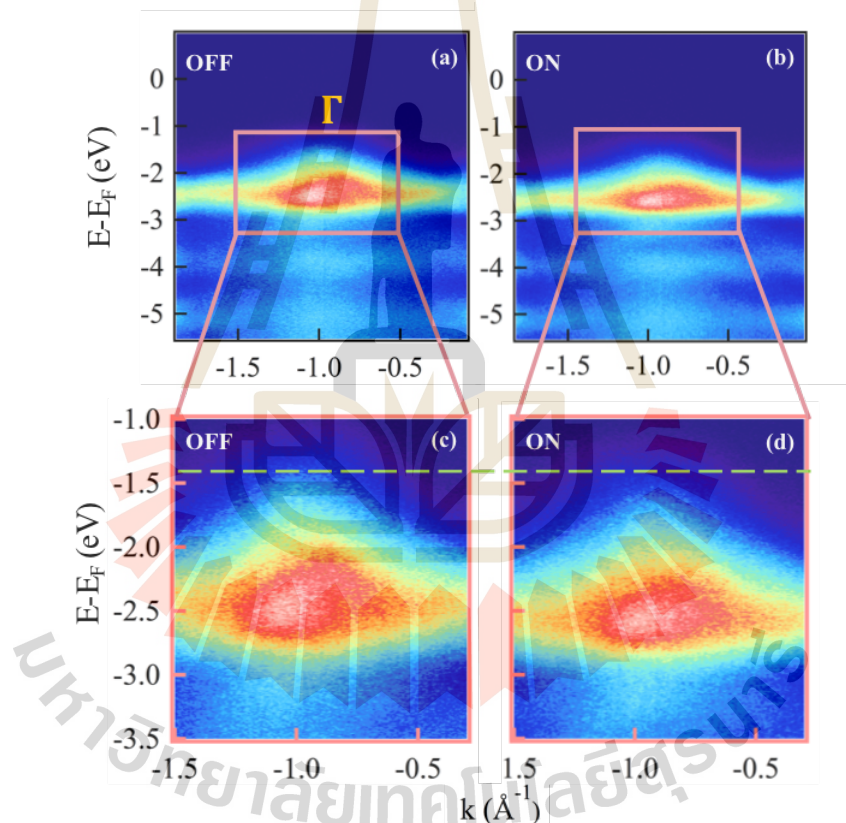
**Figure 4.1** (a) The hexagonal Brillouin zone of MoS<sub>2</sub> which consist of 3 high symmetry point,  $\Gamma$ ,  $K$  and  $M$ . (b) The valence band of MoS<sub>2</sub> at  $\Gamma$  point that was measured from ARPES.

#### 4.1.1 Shift of valence band under laser irradiation in MoS<sub>2</sub> fresh sample

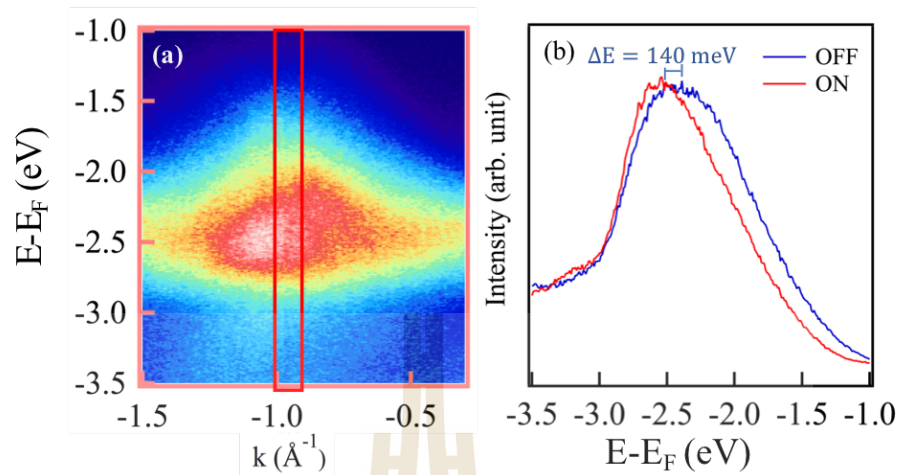
In this work, the electronic structures of MoS<sub>2</sub> samples excited by laser irradiation were studied by APRES. Figure 4.2(a) and (b) show the valence band at  $\Gamma$  point of MoS<sub>2</sub> fresh sample and valence band during the laser irradiation, respectively. Figure 4.2(c) and 4.2(d) represent the magnified ARPES images of the fresh and irradiated samples inside the rectangle region of Figure 4.2(a) and 4.2(b). From these figures, when we compare Figure 4.2(c) and (d), the shift of the valence band to higher binding energy in the irradiated sample has been observed.

We can find the magnitude of MoS<sub>2</sub> valence band shift by using energy dispersive curves (EDCs), the integration of intensities along energy scale within the red rectangle shown in Figure 4.3(a). The EDCs extracted from the fresh (blue curve)

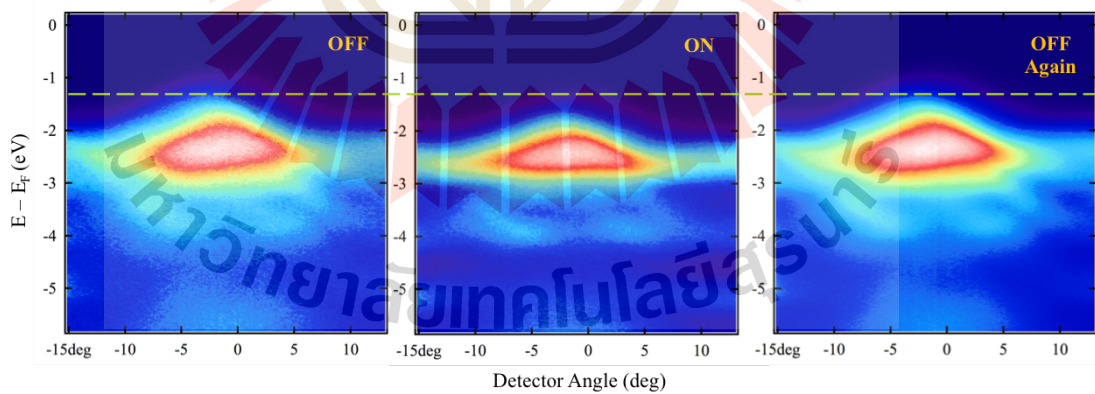
and irradiated samples (red curve) are shown in Figure 4.3(b). We found the shift of the valence band to higher binding energy was around  $140 \pm 10$  meV in the irradiated sample. As shown in Figure 4.4, the valence band was returned to the starting point when the laser was turned off again. We note that this effect can be reversible by turning on and off the laser. The shift of MoS<sub>2</sub> valence band during the laser irradiation can be explained that the electrons in the valence band were temporarily pumped to the conduction band by the excitation from laser irradiation (Sobata et al., 2012).



**Figure 4.2** (a, b) The electronic band structure near the  $\Gamma$  point of fresh and irradiated MoS<sub>2</sub> sample, respectively. (c, d) The comparison of the magnified valence band at  $\Gamma$  point of fresh and irradiated samples.



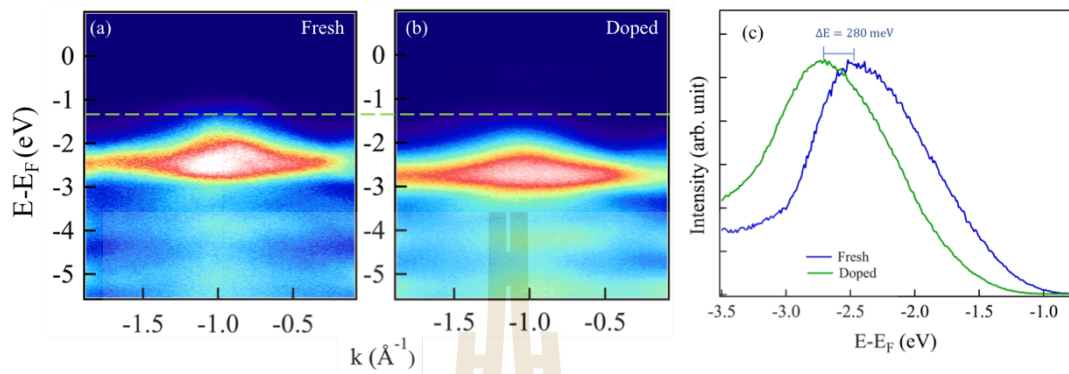
**Figure 4.3** (a) MoS<sub>2</sub> electronic structure, red rectangle indicates the region using to calculate the EDCs. (b) The extracted EDCs near the  $\Gamma$  point of MoS<sub>2</sub> between laser off and on.



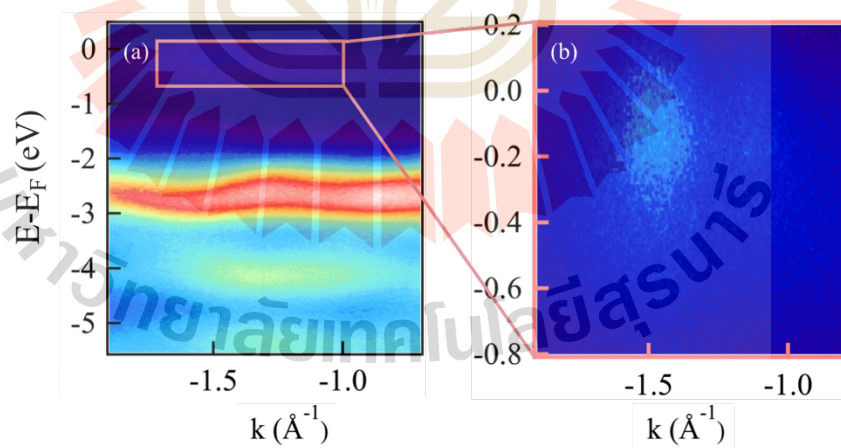
**Figure 4.4** The valence band near the  $\Gamma$  point of MoS<sub>2</sub> when the laser was switched between off and on.

#### 4.1.2 Doped MoS<sub>2</sub> sample by potassium evaporation

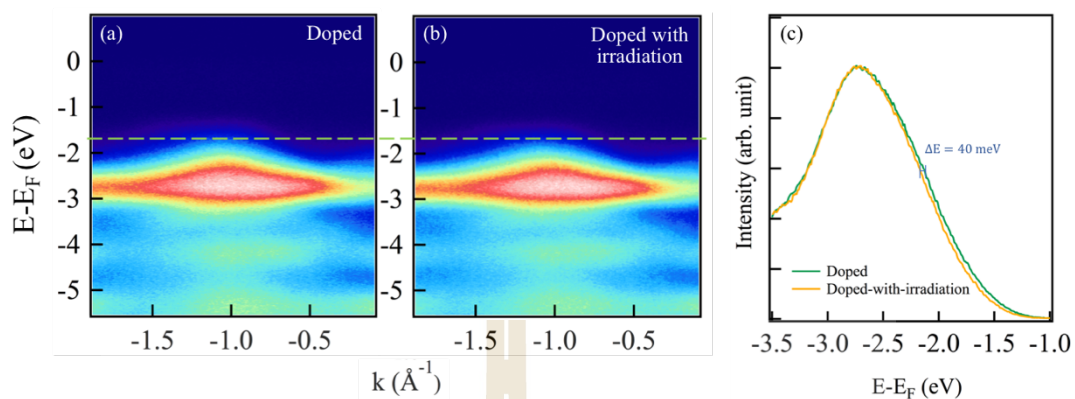
In this work, the effect of potassium evaporation at the surface of MoS<sub>2</sub> was also studied. Figure 4.5(a) and 4.5(b) show the valence band at  $\Gamma$  point of MoS<sub>2</sub> fresh and doped samples, respectively. After potassium evaporation, the shift of valence band to higher binding energy around  $280 \pm 20$  meV was observed as shown in Figure 4.5(c). As shown in Figure 4.6, the pocket of electrons was measured, which is the result of electron donation from potassium to the MoS<sub>2</sub> sample (Eknapakul et al., 2014; Fang et al., 2013). In a similar way, we also studied the effect of laser irradiation on the doped sample. The valence band of the doped with irradiation sample was shown in Figure 4.7(b). We found that the shift of the valence band with the laser irradiation was around  $40 \pm 10$  meV to higher binding energy in the doped sample, as shown in Figure 4.7(c). This result can be suggested that electrons were also pumped to the conduction band by laser irradiation in the doped MoS<sub>2</sub> sample. Figure 4.8 shows all EDC spectrum of fresh, irradiated, doped, and doped-with-irradiation samples which represent the shifts of the valence band to higher binding energy in various conditions. We found that the shift of valence band under laser irradiation is smaller than that of potassium evaporation and we also found a little bit shift in the doped sample under laser irradiation. The behaviors are the results of the optical excitation by laser and electron donation by potassium evaporation which related to the Fermi level shift (will be explained in the next section).



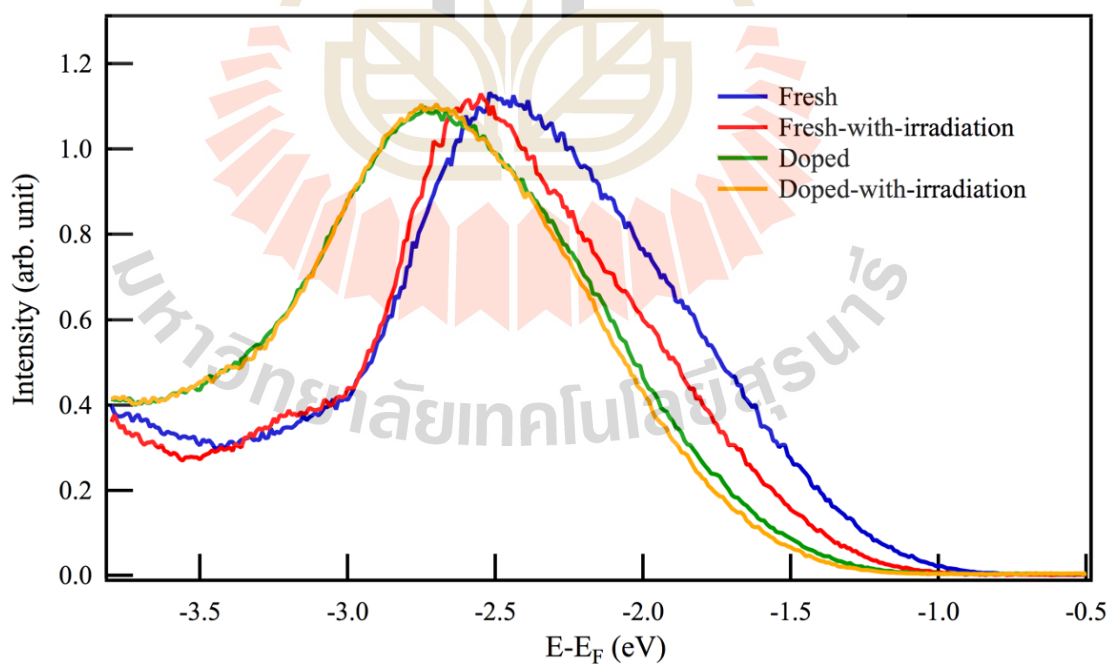
**Figure 4.5** The comparison of valence band at  $\Gamma$  point between fresh (a) and doped sample (b). (c) The comparison of EDCs between fresh and doped sample.



**Figure 4.6** The emergence of electron pocket at conduction band of the doped  $\text{MoS}_2$  sample.



**Figure 4.7** The comparison of valence band at  $\Gamma$  point between doped (a), doped-with-irradiation sample (b). (c) The comparison of EDCs between doped and doped-with-irradiation sample.

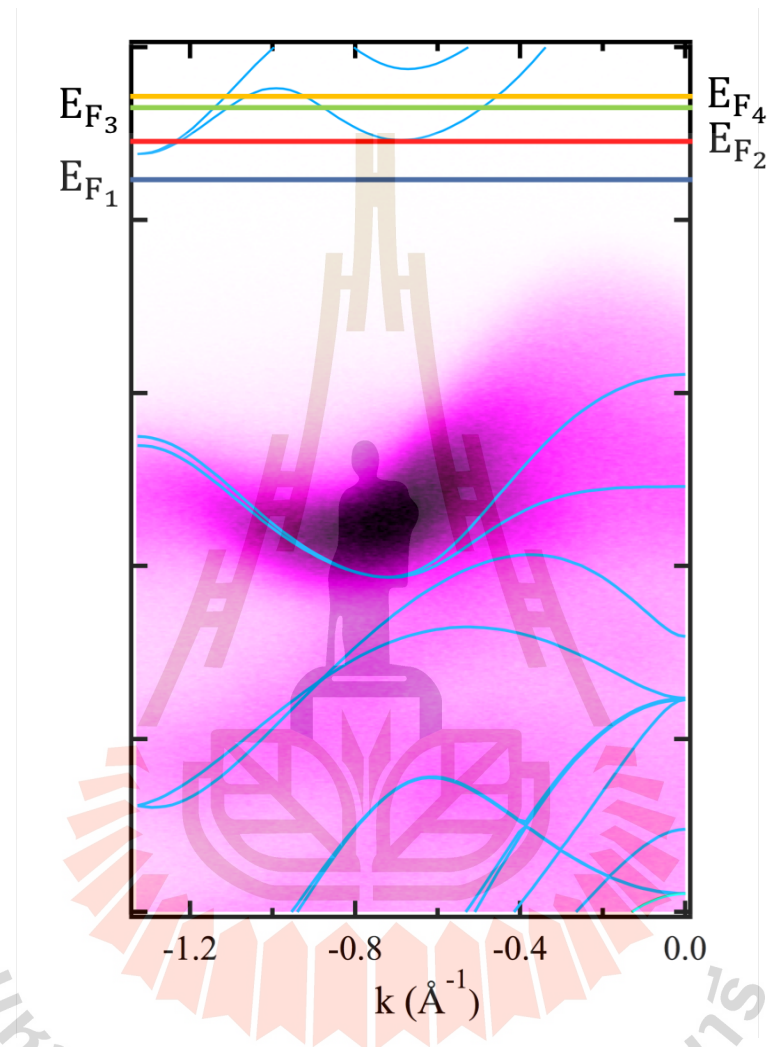


**Figure 4.8** The comparison of all EDCs between fresh, fresh-with-irradiation, doped and doped-with-irradiation  $\text{MoS}_2$  sample.

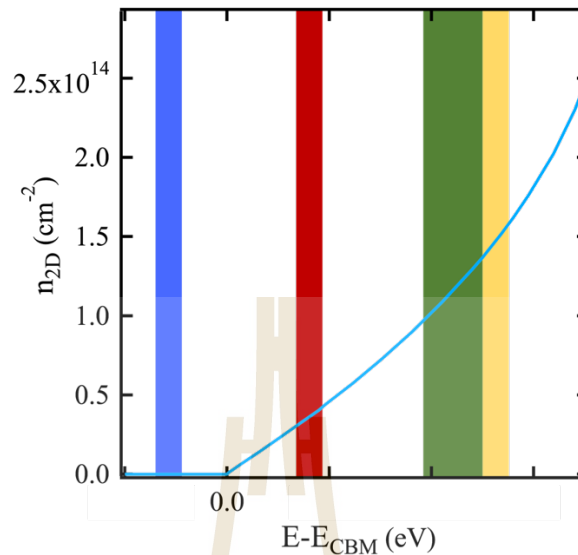


### 4.1.3 The model of MoS<sub>2</sub> band structure with different located Fermi levels.

In this section, we created the model by using the calculated MoS<sub>2</sub> band structure (from Eknapakul et al., 2014) to explain the behaviors. According to the shift of valence band, the Fermi levels of fresh, fresh-with-irradiation, doped, and doped-with-irradiation samples were assumed to locate at different energies denoted as  $E_{F1}$  to  $E_{F4}$  as shown in Figure 4.9. For the fresh sample, the Fermi level located at  $E_{F1}$  below the conduction band, which consistent with the experimental result that is seen that no state in the conduction band. This suggests that no electron has been occupied in the fresh sample. The shifts of Fermi levels above the conduction band were observed in the modified MoS<sub>2</sub> ( $E_{F2}$  to  $E_{F4}$ ). This model indicates that electrons could be accumulated at the conduction band after laser irradiation and potassium evaporation. Figure 4.10 shows the relation between the two-dimensional electron density ( $n_{2D}$ ) and the shifts of Fermi level. The calculated  $n_{2D}$  can be calculated from  $n_{2D} = g_F k_F^2 / 2\pi$  where  $k_F$  is Fermi wave vector and  $g_F=2$  which is represented by the cyan curve as a function of  $E-E_{CBM}$  in Figure 4.10. The Fermi level positions of modified MoS<sub>2</sub> were assumed to be located in the blue, red, green, and yellow regions. This suggests that the Fermi level position is related to the higher number of electron density which are the results of optical excitation and electron donation (Sobata et al., 2012; Eknapakul et al., 2014; Fang et al., 2013).



**Figure 4.9** The model of MoS<sub>2</sub> band structure with different located Fermi levels. The cyan curve represents the calculated MoS<sub>2</sub> band structure (from Eknapakul et al., 2014). The Fermi level positions of fresh, fresh-with-irradiation, doped and doped-with-irradiation sample were assumed to locate at  $E_{F1}$  to  $E_{F4}$ , respectively.

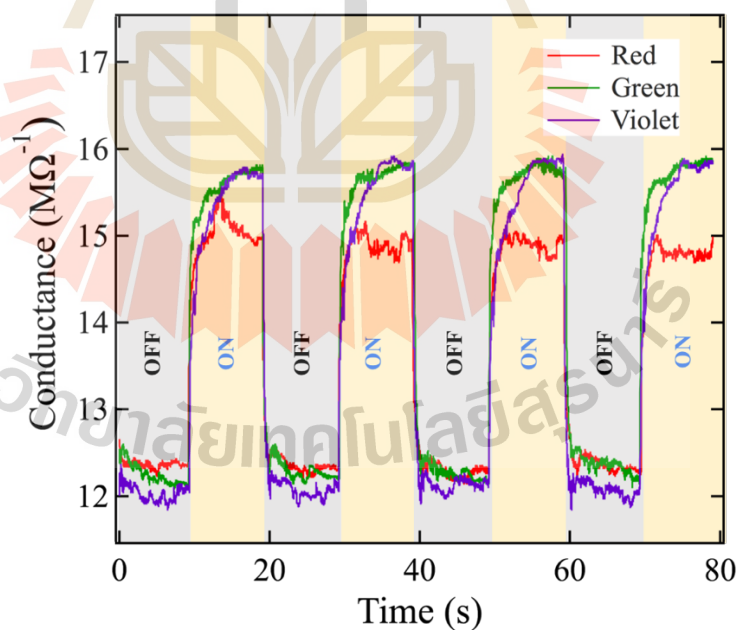


**Figure 4.10** The  $n_{2D}$  estimated from the calculated band structure (cyan curve). The Fermi levels of fresh, fresh-with-irradiation, doped and doped-with-irradiation sample are highlighted with blue, red, green, and yellow, respectively.

## 4.2 The increase of conductance measurement results

In this work, the conductance measurement of MoS<sub>2</sub> under laser irradiation was observed to support our assumption. The conductance of MoS<sub>2</sub> sample was measured by the 4-wire technique. As shown in Figure 4.11, the initial conductance was around 12 MΩ<sup>-1</sup>. After we turned on the laser, the conductance was suddenly increased to 14 MΩ<sup>-1</sup> then gradually increased to 16 MΩ<sup>-1</sup> for violet and green laser (2.75 eV and 2.33 eV, respectively) and 15 MΩ<sup>-1</sup> for red laser (1.9 eV). After the laser was turned off, the conductance was suddenly decreased to 12 MΩ<sup>-1</sup>. This process is switchable as shown in Figure 4.11. From the simple equation of conductivity is  $\sigma = ne\mu$  where  $n$  is the number of electrons,  $e$  is the charge of an electron which is constant, and  $\mu$  is electron

mobility. Hence, the conductivity is directly related to the number of electrons and the electron mobility. The ARPES results indicate that the electron can be excited to the conduction band during laser irradiation which consistent with the result of conductance increasing due to the higher number of electrons. This behavior can be described by the photoexcitation mechanism where electrons can be excited to the conduction band by irradiating photons with higher energy than the band gap of MoS<sub>2</sub> (band gap of around 1.1-1.8 eV (Bertolazzi et al., 2011; Mak et al., 2010; Li et al., 2014)). A slightly lower conductance enhancement found upon red laser irradiation may indicate that some electrons are hard to be excited if the incident energy is a little higher than the MoS<sub>2</sub> band gap. Overall, the increase of conductance in MoS<sub>2</sub> is one evidence which supports our ARPES results and the role of optical excitation.



**Figure 4.11** The switching of MoS<sub>2</sub> conductance as a function of various color laser irradiations every 10 seconds.

# CHAPTER V

## CONCLUSIONS

### 5.1 Conclusions

In this work, we study the electronic structure of MoS<sub>2</sub> under laser irradiation and potassium evaporation by using Angle-resolved Photoemission Spectroscopy (ARPES). By irradiated the violet laser on the surface of the fresh MoS<sub>2</sub> sample, the shift of valence band at  $\Gamma$  point was observed around  $140\pm 10$  meV to the higher binding energy. The shift of valence band was observed to be a switchable effect during on and off the laser. This behavior suggests that the electrons were temporarily pumped to the conduction band by optical excitation. By using potassium evaporation, the shift of valence band at  $\Gamma$  point was observed around  $280\pm 20$  meV to higher binding energy as well as the emergence of the conduction pocket. The behaviors can be explained that is the result of electron donation from potassium to MoS<sub>2</sub> sample. Moreover, the valence band shift under laser irradiation was also found in the doped MoS<sub>2</sub> sample, which is again indicated that the electrons were excited to the conduction band by using the laser in the doped sample. The model of MoS<sub>2</sub> band structure with different located Fermi levels was used to describe these behaviors. The overall mechanism related to the shift upward of Fermi level in the various conditions which are the results of optical excitation and electron donation at the surface of MoS<sub>2</sub> sample. Lastly, the increase and switchable conductance of MoS<sub>2</sub> sample under laser irradiation strongly supports the role of nonequilibrium electron pumping by optical excitation. From the properties of

conductance can be changed by light irradiation, MoS<sub>2</sub> is promising to be used in the electronic device, such as the light sensor.

## 5.2 Future direction

For the next study, we will study the more effect of light irradiation in MoS<sub>2</sub> sample. From the other results, we found that the shift of photoemission spectrum and conductance increasing are involved to the intensity of the laser, we will study the relationship between the dosing intensity and the size of the valence band shift and conductance increasing. Besides, we also found the change of MoS<sub>2</sub> work function under laser irradiation in PES measurement. Thus, we will further study the changing of its work function by laser irradiation. Moreover, MoS<sub>2</sub> consists of the valleytronics property which is the different responding to circularly polarized light at K and K' point. Therefore, the study of the effect of left and right circularly polarized light to MoS<sub>2</sub> by using ARPES would be my future plan.



**REFERENCES**

มหาวิทยาลัยเทคโนโลยีสุรนารี

## REFERENCES

- Bertolazzi, S., Brivio, J. and Kis, A. (2011). Stretching and breaking of ultrathin MoS<sub>2</sub>. **ACS nano**. 5(12): 9703-9709.
- Bhimanapati, G. R., Lin, Z., Meunier, V., Jung, Y., Cha, J., Das, S., Xiao, D., Son, Y., Strano, M. S., Cooper, V. R., Liang, L., Louie, S. G., Ringe, E., Zhao, W., Kim, S. S., Naik, R. R., Sumpter, B. G., Terrones, H., Xia, F., Wang, Y., Zhu, J., Akinwande, D., Alem, N., Schuller, J. A., Schaak, R. E., Terrones, M. and Robinson, J. A. (2015). Recent advances in two-dimensional materials beyond graphene. **ACS nano**. 9(12): 11509-11539.
- Choi, W., Choudhary, N., Han, G. H., Park, J., Akinwande, D. and Lee, Y. H. (2017). Recent development of two-dimensional transition metal dichalcogenides and their applications. **Materials Today**. 20(3): 116-130.
- Conley, H. J., Wang, B., Ziegler, J. I., Haglund Jr, R. F., Pantelides, S. T. and Bolotin, K. I. (2013). Bandgap engineering of strained monolayer and bilayer MoS<sub>2</sub>. **Nano letters**. 13(8): 3626-3630.
- Coehoorn, R., Haas, C., Dijkstra, J., Flipse, C. J. F., De Groot, R. A. and Wold, A. (1987). Electronic structure of MoSe<sub>2</sub>, MoS<sub>2</sub>, and WSe<sub>2</sub>. I. Band-structure calculations and photoelectron spectroscopy. **Physical review B**. 35(12): 6195.
- Damascelli, A. (2004). Probing the electronic structure of complex systems by ARPES. **Physica Scripta**. 2004(T109): 61.



- Dickson, R.M., Cubitt, A.B., Tsien, R.Y. and Moerner, W.E. (1997). On/off blinking and switching behaviour of single molecules of green fluorescent protein. **Nature**. 388(6640): 355.
- Eda, G., Yamaguchi, H., Voiry, D., Fujita, T., Chen, M. and Chhowalla, M. (2011). Photoluminescence from chemically exfoliated MoS<sub>2</sub>. **Nano letters**. 11(12): 5111-5116.
- Eknapakul, T., King, P. D. C., Asakawa, M., Buaphet, P., He, R. H., Mo, S. K., Takagi, H., Shen, K. M., Baumberger, F., Sasagawa, T. and Jungthawan, S. (2014). Electronic structure of a quasi-freestanding MoS<sub>2</sub> monolayer. **Nano letters**. 14(3): 1312-1316.
- Ellis, J. K., Lucero, M. J. and Scuseria, G. E. (2011). The indirect to direct band gap transition in multilayered MoS<sub>2</sub> as predicted by screened hybrid density functional theory. **Applied Physics Letters**. 99(26): 261908.
- Fang, X., Bando, Y., Liao, M., Gautam, U. K., Zhi, C., Dierre, B., Liu, B., Zhai, T., Sekiguchi, T., Koide, Y. and Golberg, D. (2009). Single-crystalline ZnS nanobelts as ultraviolet-light sensors. **Advanced Materials**. 21(20): 2034-2039.
- Fang, H., Tosun, M., Seol, G., Chang, T. C., Takei, K., Guo, J. and Javey, A. (2013). Degenerate n-doping of few-layer transition metal dichalcogenides by potassium. **Nano letters**. 13(5): 1991-1995.
- Hüfner, S. (1995). **Photoemission spectroscopy**. Berlin: Springer-Verlag.
- Hullavarad, S., Hullavarad, N., Look, D. and Claflin, B. (2009). Persistent photoconductivity studies in nanostructured ZnO UV sensors. **Nanoscale research letters**. 4(12): 1421.

- Jin, W., Yeh, P. C., Zaki, N., Zhang, D., Sadowski, J. T., Al-Mahboob, A., van Der Zande, A. M., Chenet, D. A., Dadap, J. I., Herman, I. P. and Sutter, P. (2013). Direct measurement of the thickness-dependent electronic band structure of MoS<sub>2</sub> using angle-resolved photoemission spectroscopy. **Physical review letters**. 111(10): 106801.
- Kang, M., Kim, B., Ryu, S.H., Jung, S.W., Kim, J., Moreschini, L., Jozwiak, C., Rotenberg, E., Bostwick, A. and Kim, K.S. (2017). Universal mechanism of band-gap engineering in transition-metal dichalcogenides. **Nano letters**. 17(3): 1610.
- Kang, M., Jung, S. W., Shin, W. J., Sohn, Y., Ryu, S. H., Kim, T. K., Hoesch, M. and Kim, K. S. (2018). Holstein polaron in a valley-degenerate two-dimensional semiconductor. **Nature materials**. 17(8): 676.
- King, P. D. C., He, R. H., Eknapakul, T., Buaphet, P., Mo, S. K., Kaneko, Y., Harashima, S., Hikita, Y., Bahramy, M. S., Bell, C. and Hussain, Z. (2012). Subband structure of a two-dimensional electron gas formed at the polar surface of the strong spin-orbit perovskite KTaO<sub>3</sub>. **Physical review letters**. 108(11): 117602.
- Komesu, T., Le, D., Zhang, X., Ma, Q., Schwier, E. F., Kojima, Y., Zheng, M., Iwasawa, H., Shimada, K., Taniguchi, M., Bartels, L., Rahman, T. S. and Dowben, P. A. (2014). Occupied and unoccupied electronic structure of Na doped MoS<sub>2</sub>(0001). **Applied physics letters**. 105: 241602.
- Lee, H. S., Min, S. W., Chang, Y. G., Park, M. K., Nam, T., Kim, H., Kim, J. H., Ryu, S. and Im, S. (2012). MoS<sub>2</sub> nanosheet phototransistors with thickness-modulated optical energy gap. **Nano letters**. 12(7): 3695-3700.

- Li, H., Wu, J., Yin, Z. and Zhang, H. (2014). Preparation and applications of mechanically exfoliated single-layer and multilayer MoS<sub>2</sub> and WSe<sub>2</sub> nanosheets. **Accounts of chemical research**. 47(4):1067-1075.
- Lopez-Sanchez, O., Lembke, D., Kayci, M., Radenovic, A. and Kis, A. (2013). Ultrasensitive photodetectors based on monolayer MoS<sub>2</sub>. **Nature nanotechnology**. 8(7): 497.
- Mak, K. F., Lee, C., Hone, J., Shan, J. and Heinz, T. F. (2010). Atomically thin MoS<sub>2</sub>: a new direct-gap semiconductor. **Physical review letters**. 105(13):136805.
- Mattheiss, L. F. (1973). Band structures of transition-metal-dichalcogenide layer compounds. **Physical Review B**. 8(8): 3719.
- Meevasana, W., King, P. D. C., He, R. H., Mo, S. K., Hashimoto, M., Tamai, A., Songsiriritthigul, P., Baumberger, F. and Shen, Z. X. (2011). Creation and control of a two-dimensional electron liquid at the bare SrTiO<sub>3</sub> surface. **Nature materials**. 10(2): 114.
- Nag, A., Mitra, A. and Mukhopadhyay, S. C. (2018). Graphene and its sensor-based applications: A review. **Sensors and Actuators A**. 270: 177-194.
- Nair, R. R., Blake, P., Grigorenko, A. N., Novoselov, K. S., Booth, T. J., Stauber, T., Peres, N. M. R. and Geim, A. K. (2008). Fine structure constant defines visual transparency of graphene. **Science**. 320: 1308.
- Nirmal, M., Dabbousi, B. O., Bawendi, M. G., Macklin, J. J., Trautman, J. K., Harris, T. D. and Brus, L. E. (1996). Fluorescence intermittency in single cadmium selenide nanocrystals. **Nature**. 383(6603): 802.

- Novoselov, K. S., Geim, A. K., Morozov, S. V., Jiang, D., Zhang, Y., Dubonos, S. V., Grigorieva, I. V. and Firsov, A. A. (2004). Electric field effect in atomically thin carbon films. **Science**. 306: 666-669.
- Paudel, H. (2014). **The effect of electron-hole pairs in semiconductor and topological insulator nanostructures on plasmon resonances and photon polarizations**. Ph.D. Thesis, University of Central Florida, Florida, USA.
- Pumera, M. (2011). Graphene-based nanomaterials for energy storage. **Energy & Environmental Science**. 4(3): 668-674.
- Rana, F. (n.d.). **Semiconductor Optoelectronics**. Retrieved from <https://courses.cit.cornell.edu/ece533/Lectures/handout6.pdf>.
- Riley, J. M., Meevasana, W., Bawden, L., Asakawa, M., Takayama, T., Eknapakul, T., Kim, T. K., Hoesch, M., Mo, S. K., Takagi, H. and Sasagawa, T. (2015). Negative electronic compressibility and tunable spin splitting in WSe<sub>2</sub>. **Nature nanotechnology**. 10(12): 1043.
- Sobota, J. A., Yang, S., Analytis, J. G., Chen, Y. L., Fisher, I. R., Kirchmann, P. S. and Shen, Z. X. (2012). Ultrafast optical excitation of a persistent surface-state population in the topological insulator Bi<sub>2</sub>Se<sub>3</sub>. **Physical review letters**. 108(11): 117403.
- Splendiani, A., Sun, L., Zhang, Y., Li, T., Kim, J., Chim, C. Y., Galli, G. and Wang, F. (2010). Emerging photoluminescence in monolayer MoS<sub>2</sub>. **Nano letters**. 10(4): 1271-1275.
- Suwanwong, S., Eknapakul, T., Rattanachai, Y., Masingboon, C., Rattanasuporn, S., Phatthanakun, R., Nakajima, H., King, P. D. C., Hodak, S. K. and Meevasana, W.

- (2015). The dynamics of ultraviolet-induced oxygen vacancy at the surface of insulating SrTiO<sub>3</sub> (001). **Applied Surface Science**. 355: 210-212.
- Xu, W., Liu, W., Schmidt, J.F., Zhao, W., Lu, X., Raab, T., Diederichs, C., Gao, W., Seletskiy, D.V. and Xiong, Q. (2017). Correlated fluorescence blinking in two-dimensional semiconductor heterostructures. **Nature**. 541(7635): 62-67.
- Yin, Z., Li, H., Li, H., Jiang, L., Shi, Y., Sun, Y., Lu, G., Zhang, Q., Chen, X. and Zhang, H. (2011). Single-layer MoS<sub>2</sub> phototransistors. **ACS nano**. 6(1): 74-80.
- Yin, Z., Zhu, J., He, Q., Cao, X., Tan, C., Chen, H., Yan, Q. and Zhang, H. (2013). Graphene-based materials for solar cell applications. **Advanced energy materials**. 4(1): 1300574.
- Yun, W. S., Han, S. W., Hong, S. C., Kim, I. G. and Lee, J. D. (2012). Thickness and strain effects on electronic structures of transition metal dichalcogenides: 2H-MX<sub>2</sub> semiconductors (M= Mo, W; X= S, Se, Te). **Physical Review B**. 85(3): 033305.
- Zhang, R., Tsai, I. L., Chapman, J., Khestanova, E., Waters, J., and Grigorieva, I. V. (2016). Superconductivity in potassium-doped metallic polymorphs of MoS<sub>2</sub>. **Nano letters**. 16(1): 629-636.

## CURRICULUM VITAE

**Name** Ms. Pakwan Chanprakhon

**Date of Birth** December 6<sup>th</sup>, 1994 in Buriram, Thailand

**Place of Birth** Thai

**E-mail** pakwan.rin@gmail.com

### Education

2013-2016 B.Sc. (Physics), Suranaree University of Technology, Thailand

2017-present M.Sc. (Physics), Suranaree University of Technology, Thailand

### Oral presentation:

**Chanprakhon, P.**, Eknapakul, T., Thila, S., Polin, S., Nakajima, H., Rattanachatta, A., and Meevasana, W. (2019). Optical Excitation and Electron Donation at the surface of MoS<sub>2</sub>, Presented at The 2<sup>nd</sup> Materials Research Society of Thailand International Conference, Thailand (2019-07-10 - 2019-07-12).

มหาวิทยาลัยเทคโนโลยีสุรนารี